SUPPORTING INFORMATION

Intramolecular through-space heavy-atom effect in multiresonant thermally activated delayed fluorescence emitters with [2.2]paracyclophane

Yan Xu[a‡], *Hassan Hafeez*[b‡], *Wenrui Wang*[a], *Ifor D. W. Samuel*[b*], *Eli Zysman-Colman*[a*]

[a] Organic Semiconductor Centre, EaStCHEM School of Chemistry, University of St Andrews, St Andrews, Fife, UK, KY16 9ST, E-mail: eli.zysman-colman@st-andrews.ac.uk

[b] Organic Semiconductor Centre, SUPA School of Physics and Astronomy, University of St Andrews, St Andrews, Fife, UK, KY16 9SS, E-mail: idws@st-andrews.ac.uk

[‡]Yan Xu and Hassan Hafeez contributed equally to this work.

Table of Contents

1. General methods

General synthetic procedures

1^2-bromo-1,4(1,4)-dibenzenacyclohexaphane (**PCP-Br**),[1] $1^2,4^3$-dibromo-1,4(1,4)-dibenzenacyclohexaphane (**pseudo-*ortho*-PCP-2Br, *po*-PCP-2Br)**,[2] $1^2,4^2$-dibromo-1,4(1,4)-dibenzenacyclohexaphane (**pseudo-*meta*-PCP-2Br, *pm*-PCP-2Br**),[2] and ***t*CzBN-Bpin**[3] were synthesized according to literature procedures. All other reagents and solvents were obtained from commercial sources and used as received. Air-sensitive reactions were performed under a nitrogen atmosphere using Schlenk techniques. Anhydrous THF used in the reaction were obtained from a MBRAUN SPS5 solvent purification system. Flash column chromatography was carried out using a Teledyne ISCO CombiFlash® NextGen 300+ system with RediSep® Normal-Phase Silica columns in sizes of 40 g silica packing. Analytical thin-layer-chromatography (TLC) was performed with silica plates with aluminum backings (250 μm with F-254 indicator). TLC visualization was accomplished by 254/365 nm UV lamp. HPLC analysis was conducted on a Shimadzu LC-40 HPLC system. HPLC traces were performed using a Shim-pack GIST 3μm C18 reverse phase analytical column. ^{1}H and ^{13}C NMR spectra were recorded on a Bruker Advance spectrometer (500 MHz for ^{1}H, 126 MHz for ^{13}C) in $CDCl_3$. The following abbreviations have been used for multiplicity assignments: “s” for singlet, “d” for doublet, “dd” for doublet of doublets, “dt” for doublet of triplets, “td” for triplet of doublets, “ddd” for doublet of doublet of doublets, “m” for multiplet. ^{1}H and ^{13}C NMR spectra were referenced to residual solvent peaks. Melting points were measured using open-ended capillaries on an Electrothermal 1101D Mel-Temp apparatus and are uncorrected. High-resolution mass spectrometry (HRMS) measurements were performed at the University of Edinburgh Mass Spectrometry Facility on a micrOTOF, and elemental analyses (EA) were performed at the London Metropolitan University by O. McCullough.

Electrochemistry measurements

Cyclic Voltammetry (CV) analyses were performed on an Electrochemical Analyzer

potentiostat model 620E from CH Instruments at a sweep rate of 100 mV/s. Differential Pulse Voltammetry (DPV) analyses were carried out on the same instrument, with an increment potential of 0.004 V and a pulse amplitude, width, and period of 50 mV, 0.06 s, and 0.5 s, respectively. Samples were prepared in DCM and degassed by sparging with DCM-saturated nitrogen gas for 5 minutes before measurements. All measurements were performed in 0.1 M DCM solution of tetra-*n*-butylammonium hexafluorophosphate, [^{n}Bu$_4$N]PF$_6$, which was used as the supporting electrolyte. An Ag/Ag$^+$ electrode was used as the reference electrode while a glassy carbon electrode and a platinum wire were used as the working electrode and counter electrode, respectively. The redox potentials are reported relative to a saturated calomel electrode (SCE) with a ferrocene/ferrocenium (Fc/Fc$^+$) redox couple as the internal standard (0.46 V vs SCE for DCM).[4] The HOMO and LUMO energies were determined using the relation $E_{HOMO/LUMO} = -(E_{ox} / E_{red} + 4.8)$ eV, where E_{ox} and E_{red} are the onset of anodic and cathodic peak potentials, respectively calculated from DPV relative to Fc/Fc$^+$.[5]

Theoretical calculations

Density functional theory (DFT) and TD(A)-DFT calculations were performed using the Gaussian 16 revision C.01 package.[6] The ground-state optimization was carried out using DFT using the PBE0[7] functional, the 6-31G(d,p) basis set[8] in the gas phase, starting from a structure drawn and optimized using Chem3D. The vertical excited-state calculations were performed using Time-Dependent DFT within the Tamm-Dancoff approximation (TDA-DFT),[9] with the same functional and basis set as for the ground-state geometry optimization in the gas phase. Spin-orbit coupling matrix elements SOCME were calculated based on the optimized triplet excited state geometry using PySOC.[10] The molecular orbital distributions were visualized with Gaussview 6.0.[11] Wavefunction calculations were performed using the Turbomole 7.5 package[12, 13] using the resolution of the identity approximation.[14] The spin-component scaling (SCS) modification was applied to all calculations.[15] Vertical excited state calculations using SCS-ADC(2)[16, 17] with cc-pVDZ basis set[18] were performed on the DFT optimized ground state geometry with the first two singlet states[19] and first two triplet states[20, 21] calculated. Calculations were submitted and processed using the Digichem software package (version 6),[22,

[23] which incorporates a number of publicly available software libraries, including: cclib[24] for parsing of result files, VMD[25]/Tachyon[26] for 3D rendering, Matplotlib for drawing of graphs[27], Open Babel[28]/Pybe[29] file interconversion.

Photophysical measurements

Optically dilute solutions of concentrations on the order of 10^{-5} or 10^{-6} M were prepared in spectroscopic or HPLC grade toluene for absorption and emission analysis. Absorption spectra were recorded at room temperature on a Shimadzu UV-2600 double-beam spectrophotometer with a 1 cm quartz cuvette. Molar absorptivity determination was verified by a linear regression analysis of values obtained from five independent solutions at varying concentrations ranging from 2.81×10^{-6} to 1.53×10^{-5} M for **PCP-*t*CzBN**, 2.47×10^{-6} to 1.34×10^{-5} M for ***po*-PCP-*t*CzBN-Br** and 2.98×10^{-6} to 1.62×10^{-5} M for ***pm*-PCP-*t*CzBN-Br**, with absorbance ranging from 0.151 to 0.820 for **PCP-*t*CzBN**, 0.079 to 0.443 for ***po*-PCP-*t*CzBN-Br** and 0.082 to 0.464 for ***pm*-PCP-*t*CzBN-Br**.

For emission studies, aerated solutions, steady-state PL and excitation spectra and time-resolved PL measurements were recorded at room temperature using an Edinburgh Instruments FS5 fluorimeter. Samples were excited at 325 nm for steady-state PL measurements and 375 nm for time-resolved PL decays. Aerated solution-state samples were prepared by bubbling solutions with compressed air for 5 minutes and spectra were measured using the cuvette for absorption analysis. Degassed solutions were prepared via three freeze-pump-thaw cycles and spectra were measured using a home-made Schlenk quartz cuvette. Photoluminescence quantum yields (Φ_{PL}) for solutions were determined using the optically dilute method[30] in which four sample solutions with absorbances of ca. 0.09, 0.07, 0.04 and 0.02 at 450 nm for ***po*-PCP-*t*CzBN-Br** and 0.10, 0.08, 0.05 and 0.03 at 450 nm for ***pm*-PCP-*t*CzBN-Br** were used. The Beer-Lambert law was found to remain linear across the concentrations of the solutions. For each sample, linearity between absorption and emission intensity was verified through linear regression analysis with the Pearson regression factor (R^2) for the linear fit of the data set surpassing 0.9. Individual relative quantum yield values were calculated for each solution and the values reported represent the slope obtained from the linear fit of these results. The Φ_{PL} was

determined using the equation $\Phi_{PL} = (\Phi_r * \frac{A_r}{A_s} * \frac{I_s}{I_r} * \frac{n_s^2}{n_r^2})$, where A stands for the absorbance at the excitation wavelength (λ_{exc}: 450 nm), I is the integrated area under the corrected emission curve and n is the refractive index of the solvent with the subscripts "s" and "r" representing sample and reference respectively. Φ_r is the absolute PL quantum yield of the external reference, $[Ru(bpy)_3]Cl_2$ (Φ_r = 2.8% in aerated water).[31] The experimental uncertainty in the Φ_{PL} is conservatively estimated to be 10%, though we have found that statistically we can reproduce Φ_{PL} values to within 3% relative error.

For solid-state film measurements, the 2, 5 and 10 wt% doped films of emitters in a host matrix, 98, 95 and 90% w/w (9.8, 9.5 and 9.0 mg) of host was dissolved in 900 μL of solvent and to this, 2, 5 and 10% w/w (0.2, 0.5 and 1.0 mg emitter in 100 μL of solvent) of emitter was added. Thin films were then spin-coated onto a sapphire substrate using a spin speed of 2000 rpm for 60 s and annealed at 80 °C for 60 s to obtain a thickness of ~80 nm. An integrating sphere (Edinburgh Instruments FS5, SC30 module) was employed for the photoluminescence quantum yield measurements of thin film samples. The Φ_{PL} of the films were then measured in air and in N_2 by purging the integrating sphere with N_2 gas flow for 2 min. The photophysical properties of the film samples were measured using an Edinburgh Instruments FS5 fluorimeter. Time-resolved PL decays of the thin films were carried out using time-correlated single-photon counting (TCSPC) mode for short-time range (1 ns-100 ns) and excited at 375 nm by a 5 mW EPL-375 picosecond pulsed diode laser. The long-time range (1 ns-400 μs, 1 ns-2 ms) of PL decays and were excited at 375 nm and measured using a 5 W pulsed xenon microsecond flash lamp by the multi-channel scaling (MCS) mode. The samples were kept in a vacuum of $< 8 \times 10^{-4}$ mbar.

The singlet and triplet state energies in 2-MeTHF glass and in doped film were determined from the onset values of the steady-state PL (SS PL) and delayed emission spectra at 77 K. The singlet-triplet energy gap (ΔE_{ST}) was estimated from the difference in energy of the onsets of these spectra. For SS PL, samples were excited by a xenon lamp emitting at 340 nm. For phosphorescence spectra, samples were excited by a xenon flashlamp emitting at 340 nm (EI FS5, SC-70). Phosphorescence spectra were measured with a time-gated window of 1-10 ms with xenon flashlamp operating at 100 Hz.

Fitting of time-resolved luminescence measurements

Time-resolved PL measurements were fitted to a sum of exponential decay model, with chi-squared (χ^2) values between 1 and 2, using the Fluoracle software. Each component of the decay is assigned a weight, (w_i), which is the contribution of the emission from each component to the total emission. The average lifetime was then calculated using the following:

For two exponential decay model:

$\tau_{AVG}=\tau_1 w_1+\tau_2 w_2$

with weights defined as $w_1 = \frac{A_1\tau_1}{A_1\tau_1+A_2\tau_2}$ and $w_2 = \frac{A_2\tau_2}{A_1\tau_1+A_2\tau_2}$, where A_1 and A_2 are the preexponential-factors of each component.

For three exponential decay model:

$\tau_{AVG}=\tau_1 w_1+\tau_2 w_2+\tau_3 w_3$

with weights defined as $w_1 = \frac{A_1\tau_1}{A_1\tau_1+A_2\tau_2+A_3\tau_3}$, $w_2 = \frac{A_2\tau_2}{A_1\tau_1+A_2\tau_2+A_3\tau_3}$ and $w_3 = \frac{A_3\tau_3}{A_1\tau_1+A_2\tau_2+A_3\tau_3}$, where A_1, A_2 and A_3 are the preexponential-factors of each component.

OLED Fabrication and Characterization

The bottom-emitting OLEDs were fabricated using pre-patterned indium tin oxide (ITO) on a glass substrate. The substrate was cleaned with acetone then isopropanol for 30 min each, using an ultrasonication bath set at 60 °C. The OLEDs were fabricated using a thermal evaporator (Angstrom Engineering, USA) under a high vacuum with a base pressure of around 3×10^{-7} mbar. The substrate was loaded into the thermal evaporator using a custom-made air-tight metal container to avoid dust particles and contamination. All organic layers were deposited on the ITO anode with evaporation rates between 0.3-0.6 Å/s. This was followed by lithium fluoride (LiF) and aluminum (Al) deposition at the rates of 0.05 Å/s and 2 Å/s, respectively. The fabricated OLEDs were encapsulated in an N_2 atmosphere using glass that was cleaned using the same method mentioned above for the substrate. A UV-curable epoxy resin (NOA 68) was used to ensure an air-tight attachment of the encapsulation with the substrate. The active (emission) area of the OLEDs was 2 mm^2. The fabricated OLEDs were measured for their

current-voltage-luminance characteristics using a Keithley 2400 power source meter and a custom-made photodiode system connected to a Keithley 2000 multimeter. The electroluminescence spectra of the devices were analyzed using a CCD (Andor DV420-BV) spectrometer.

2. Experimental section

Synthesis of PCP-*t*CzBN

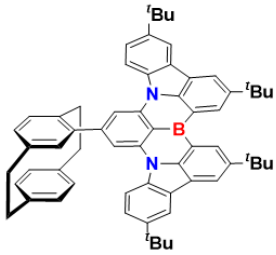

Under a N_2 atmosphere, a mixture of **PCP-Br** (169.0 mg, 0.6 mmol, 1.5 equiv.), ***t*CzBN-Bpin** (300.0 mg, 0.4 mmol, 1 equiv.), $Pd(PPh_3)_4$ (23.0 mg, 19.6 μmol, 0.05 equiv.), 2 M Na_2CO_3 (0.5 mL) and THF (10 mL) were combined. The reaction mixture was heated to reflux and stirred for 12 h. The reaction mixture was cooled to room temperature and the product was filtered and washed with water (3 × 50 mL) and dichloromethane (3 × 30 mL). The crude mixture was purified by silica gel flash column chromatography using dichloromethane:petroleum ether = 1:10 as eluent to afford the desired compound as yellow solid product. **Yield**: 53%. **Mp**: 289-291 °C (Lit. Mp:[32] 289-291 °C). **R_f**: 0.5 (dichloromethane:petroleum ether = 1:5). **^{1}H NMR (500 MHz, $CDCl_3$) δ (ppm)**: 9.17 (d, *J* = 1.9 Hz, 2H), 8.53- 8.48 (m, 4H), 8.45 (s, 2H), 8.31 (d, *J* = 2.0 Hz, 2H), 7.70 (dd, *J* = 8.7, 2.1 Hz, 2H), 6.99 (dd, *J* = 7.7, 1.8 Hz, 1H), 6.94-6.87 (m, 2H), 6.81-6.75 (m, 2H), 6.69 (td, *J* = 7.5, 1.8 Hz, 2H), 3.83 (ddd, *J* = 13.8, 10.0, 3.9 Hz, 1H), 3.42-3.34 (m, 1H), 3.31-3.17 (m, 4H), 2.95 (ddd, *J* = 13.8, 10.1, 3.8 Hz, 1H), 2.82 (ddd, *J* = 13.9, 10.0, 4.8 Hz, 1H), 1.70 (s, 18H), 1.55 (s, 18H). **^{13}C NMR (126 MHz, $CDCl_3$) δ (ppm)**: 146.4, 145.5, 144.8, 144.6, 142.6, 141.9, 140.3, 140.1, 139.8, 138.5, 137.7, 136.5, 133.7, 133.2, 133.0, 132.7, 131.9, 130.3, 130.0, 127.3, 124.6, 123.7, 122.0, 121.9, 120.8, 117.6, 114.0, 109.8, 35.9, 35.6, 35.4, 35.3, 35.0, 34.7, 32.4, 32.0. **HR-MS $[M+H]^+$ Calculated ($C_{62}H_{64}BN_2$):** 847.5157; **Found:** 847.5166. **EA calculated:** ($C_{62}H_{63}BN_2$) C, 87.92%; H, 7.50%; N, 3.31%. **Found:** C, 87.50%; H, 7.69%; N, 2.98%. **HPLC purity:** > 99% (retention time: 13.263 minutes, employing an eluent of 100% THF). The analytical data match those found in the literature.[32]

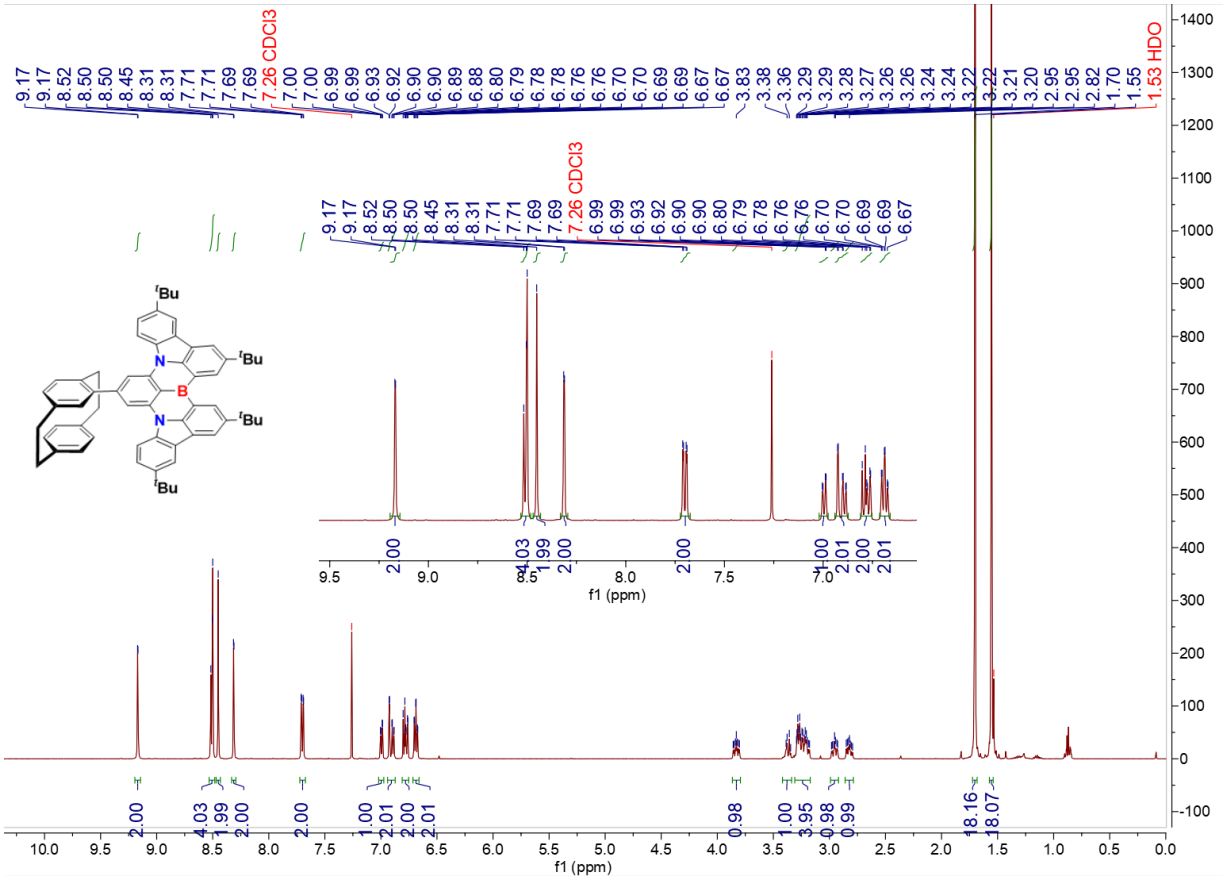

Figure **S1**. ^{1}H-NMR spectrum of **PCP-*t*CzBN** in $CDCl_3$

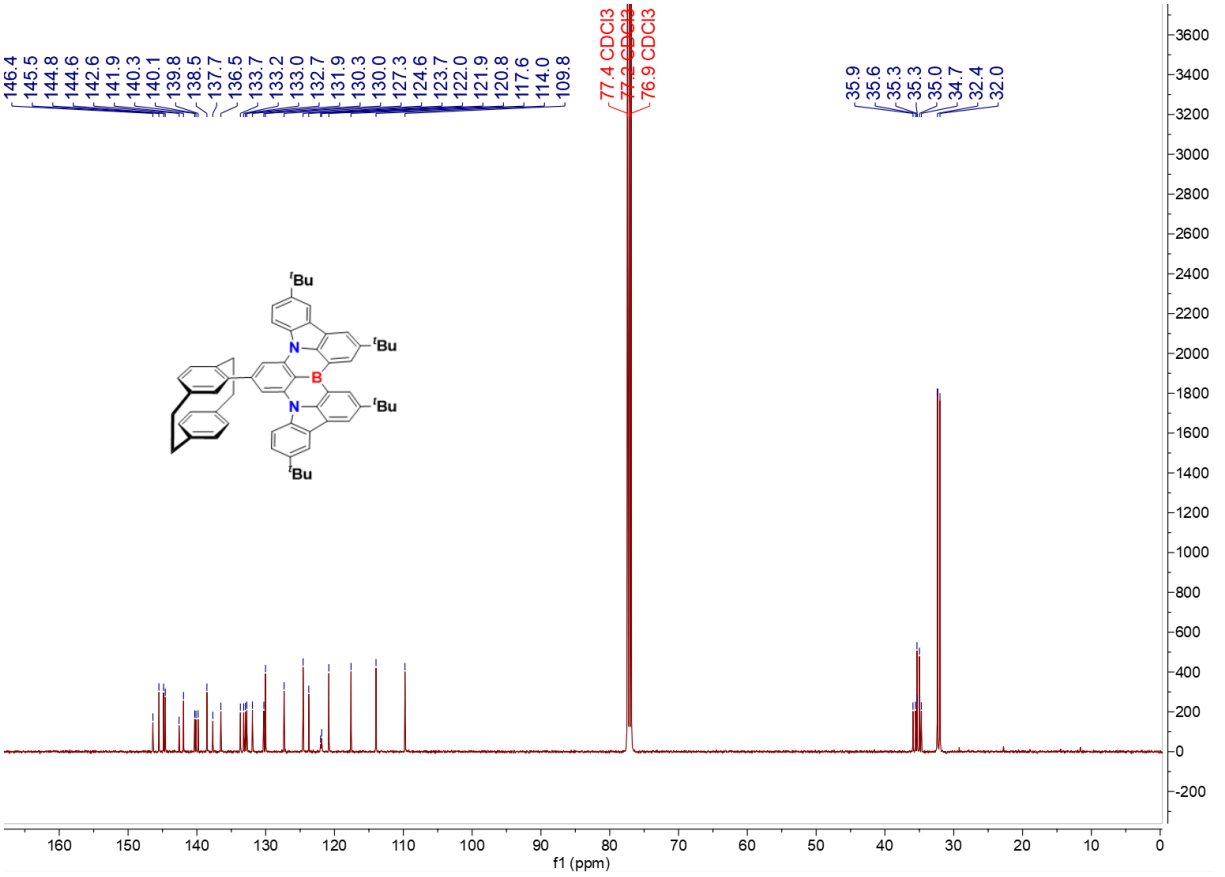

Figure **S2**. ^{13}C-NMR spectrum of **PCP-*t*CzBN** in $CDCl_3$

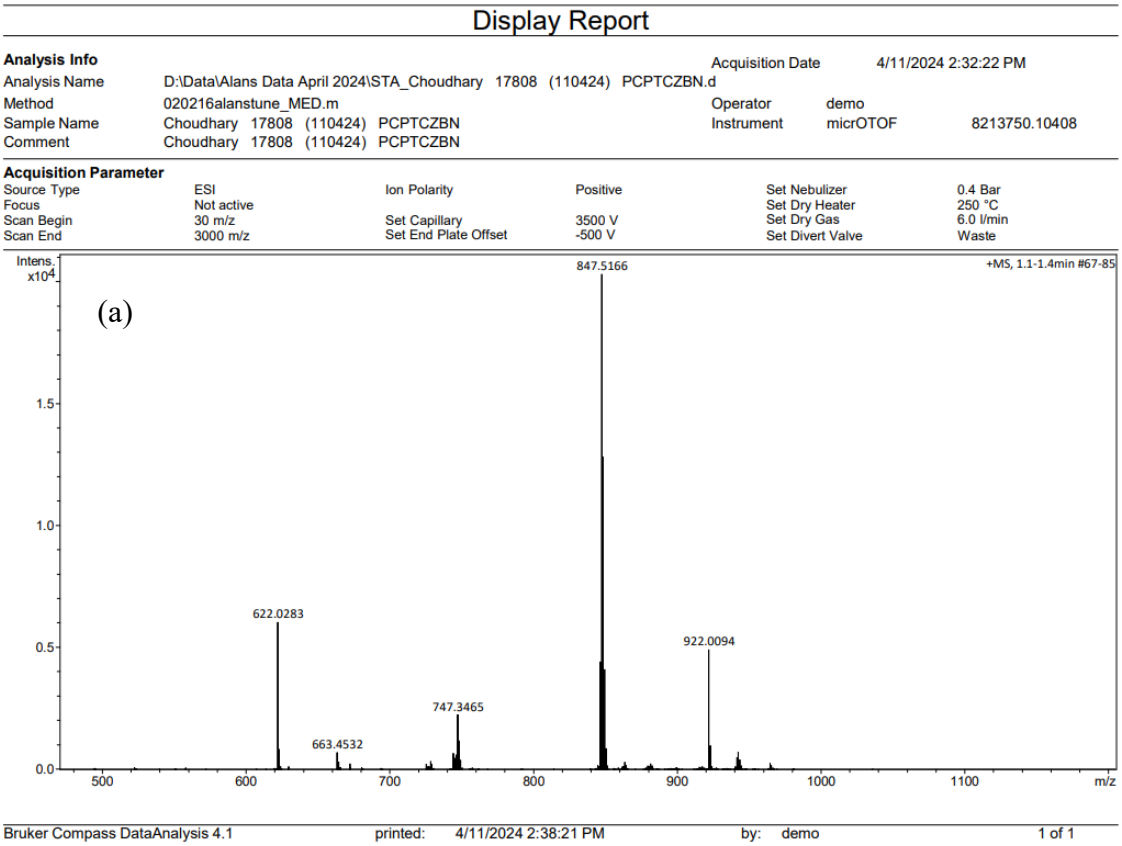

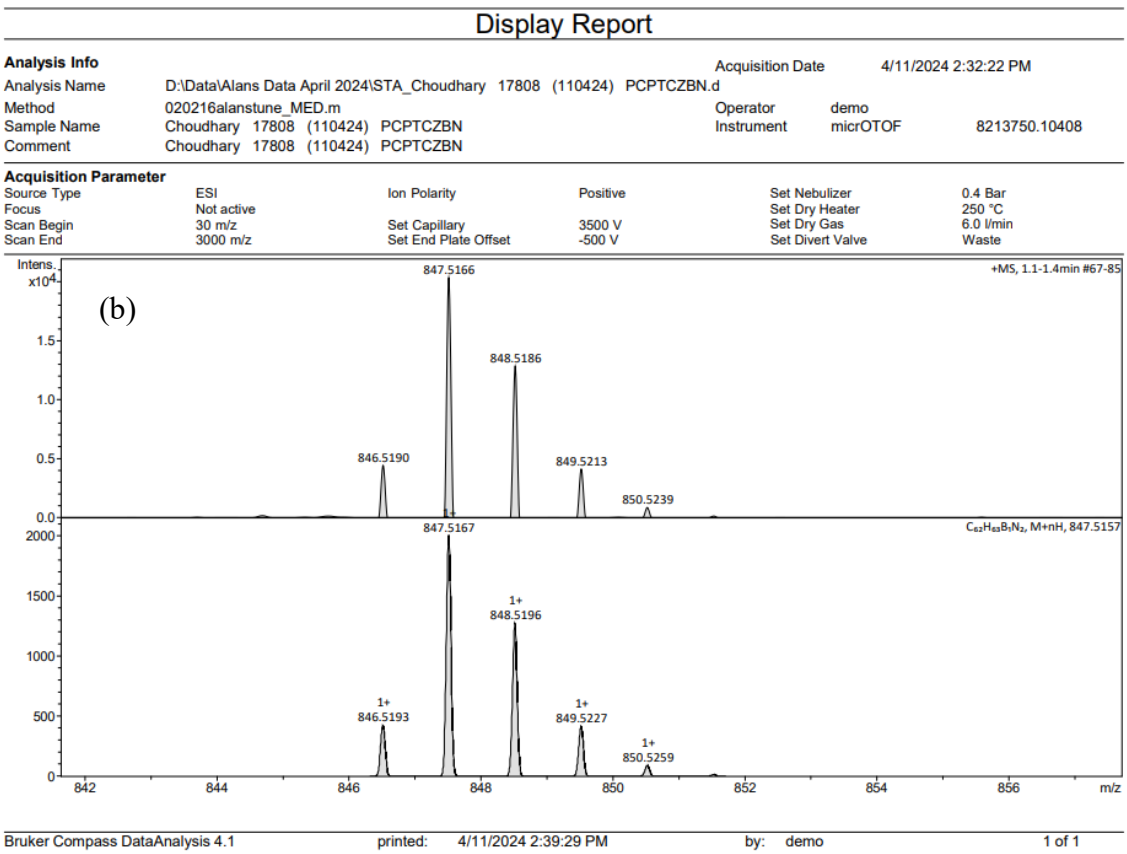

Figure **S3**. HRMS of **PCP-*t*CzBN** (a) full spectrum and (b) **[M+H]**$^+$ ($C_{62}H_{64}BN_2$).

<Chromatogram>

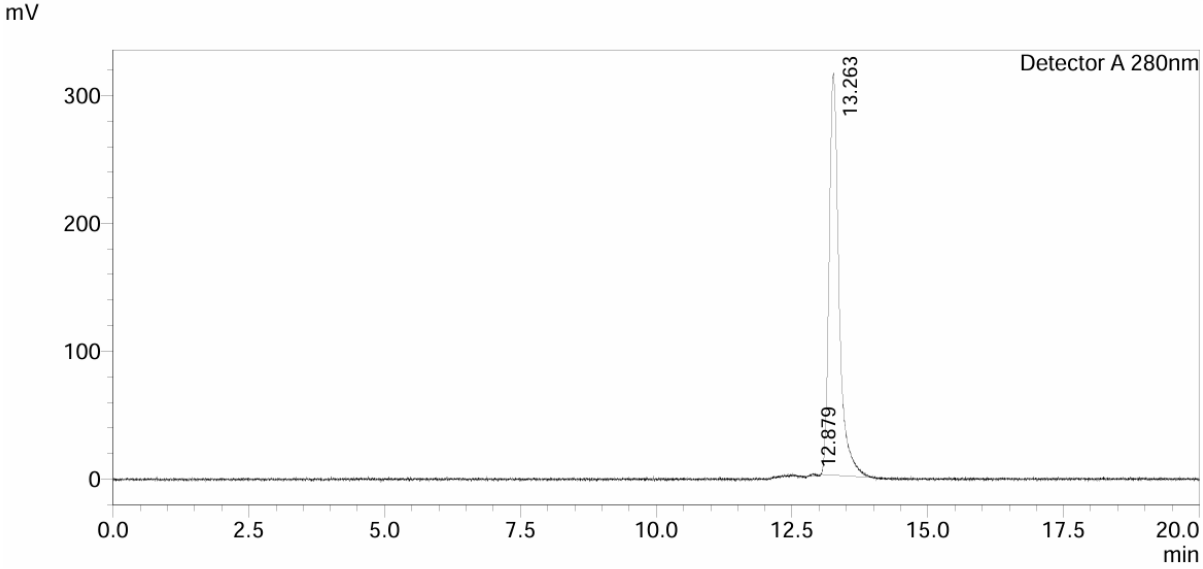

<Peak Table>

Detector A 280nm

Peak#	Ret. Time	Area	Height	Area%	Area/Height	Width at 5% Height
1	12.879	5155	1462	0.128	3.525	0.092
2	13.263	4013038	313586	99.872	12.797	0.496
Total		4018193	315048	100.000		

Figure **S4**. HPLC spectrum of **PCP-*t*CzBN**

LONDON METROPOLITAN UNIVERSITY
HUMAN SCIENCES

Elemental Analysis Sample Results

Name	Yan Xu
Organisation Name	University of St Andrews
Purchase order number	

Standard – Acetanilide		
Element	**Expected %**	**Found**
Carbon	71.10 (+/- 0.23)	71.02
Hydrogen	6.71 (+/- 0.07)	6.64
Nitrogen	10.34 (+/- 0.09)	10.29

Analysis – TSCT2			
Element	**Expected %**	**Found (1)**	**Found (2)**
Carbon	87.92	87.51	87.48
Hydrogen	7.50	7.65	7.72
Nitrogen	3.31	2.88	3.08

Date completed	16.04.2024
Signature	O. McCullough
Comments	

Figure **S5**. EA results for **PCP-*t*CzBN**

Synthesis of *po*-PCP-*t*CzBN-Br

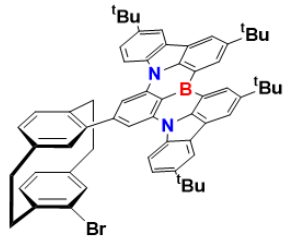

Under a N_2 atmosphere, a mixture of ***po*-PCP-2Br** (215.0 mg, 0.6 mmol, 1.5 equiv.), ***t*CzBN-Bpin** (300.0 mg, 0.4 mmol, 1 equiv.), $Pd(PPh_3)_4$ (23.0 mg, 19.6 μmol, 0.05 equiv.), 2 M Na_2CO_3 (0.5 mL) and THF (10 mL) were combined. The reaction mixture was heated to reflux and stirred for 12 h. The reaction mixture was cooled to room temperature and the product was filtered and washed with water (3 × 50 mL) and dichloromethane (3 × 30 mL). The crude mixture was purified by silica gel flash column chromatography using dichloromethane:petroleum ether = 1:10 as eluent to afford the desired compound as yellow solid product. **Yield**: 46%. **Mp**: 284-287 °C. **R*f***: 0.5 (dichloromethane: petroleum ether = 1:5). **^{1}H NMR (500 MHz, $CDCl_3$) δ (ppm)**: 9.15 (d, *J* = 1.9 Hz, 2H), 8.64 (d, *J* = 8.8 Hz, 2H), 8.53 (s, 2H), 8.49 (d, *J* = 1.8 Hz, 2H), 8.28 (d, *J* = 2.0 Hz, 2H), 7.66 (dd, *J* = 8.8, 2.1 Hz, 2H), 7.60 (d, *J* = 1.8 Hz, 1H), 6.87 (d, *J* = 7.7 Hz, 1H), 6.77-6.69 (m, 3H), 6.64 (dd, *J* = 7.7, 1.8 Hz, 1H), 3.93-3.85 (m, 1H), 3.67 (dd, *J* = 13.6, 9.4 Hz, 1H), 3.40 (dt, *J* = 13.6, 8.7 Hz, 1H), 3.35-3.27 (m, 1H), 3.11 (ddd, *J* = 13.7, 10.1, 6.5 Hz, 1H), 3.01-2.85 (m, 2H), 2.50 (ddd, *J* = 13.4, 9.9, 6.5 Hz, 1H), 1.69 (s, 18H), 1.54 (s, 18H). **^{13}C NMR (126 MHz, $CDCl_3$) δ (ppm)**: 145.8, 145.5, 144.8, 144.7, 142.0, 142.0, 141.9, 139.7, 139.3, 138.3, 137.3, 136.7, 135.0, 134.6, 133.3, 131.6, 129.9, 128.9, 127.1, 126.6, 124.5, 123.8, 122.4, 121.8, 120.8, 117.3, 114.9, 109.4, 36.6, 35.4, 35.3, 35.0, 34.2, 32.6, 32.4, 32.0. **HR-MS $[M]^+$ Calculated ($C_{62}H_{62}BBrN_2$):** 924.42; **Found:** 924.42. **EA calculated:** ($C_{62}H_{62}BBrN_2$) C, 80.43%; H, 6.75%; N, 3.03%. **Found:** C, 80.22%; H, 6.85%; N, 2.79%. **HPLC purity:** > 99% (retention time: 13.271 minutes, employing an eluent of 100% THF)

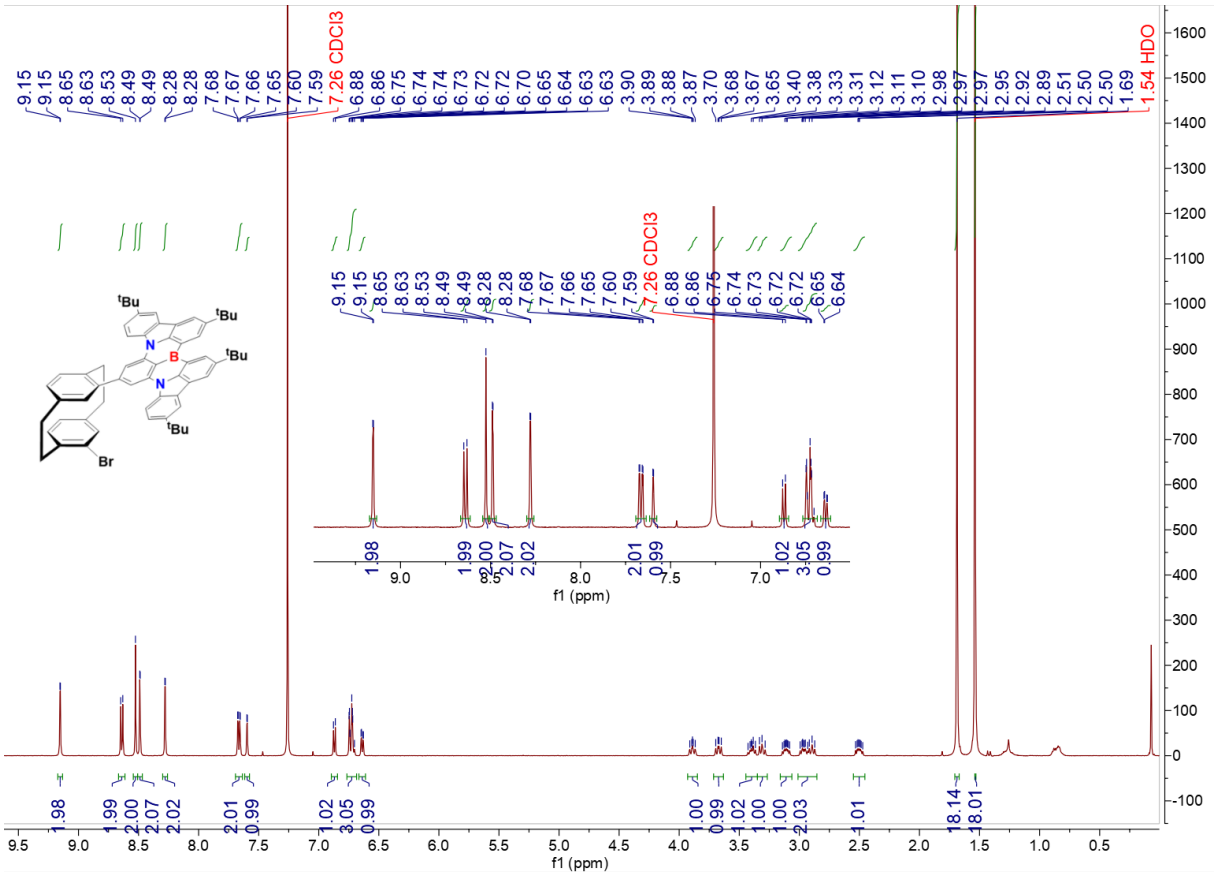

Figure **S6**. ^{1}H-NMR spectrum of ***po*-PCP-*t*CzBN-Br** in $CDCl_3$.

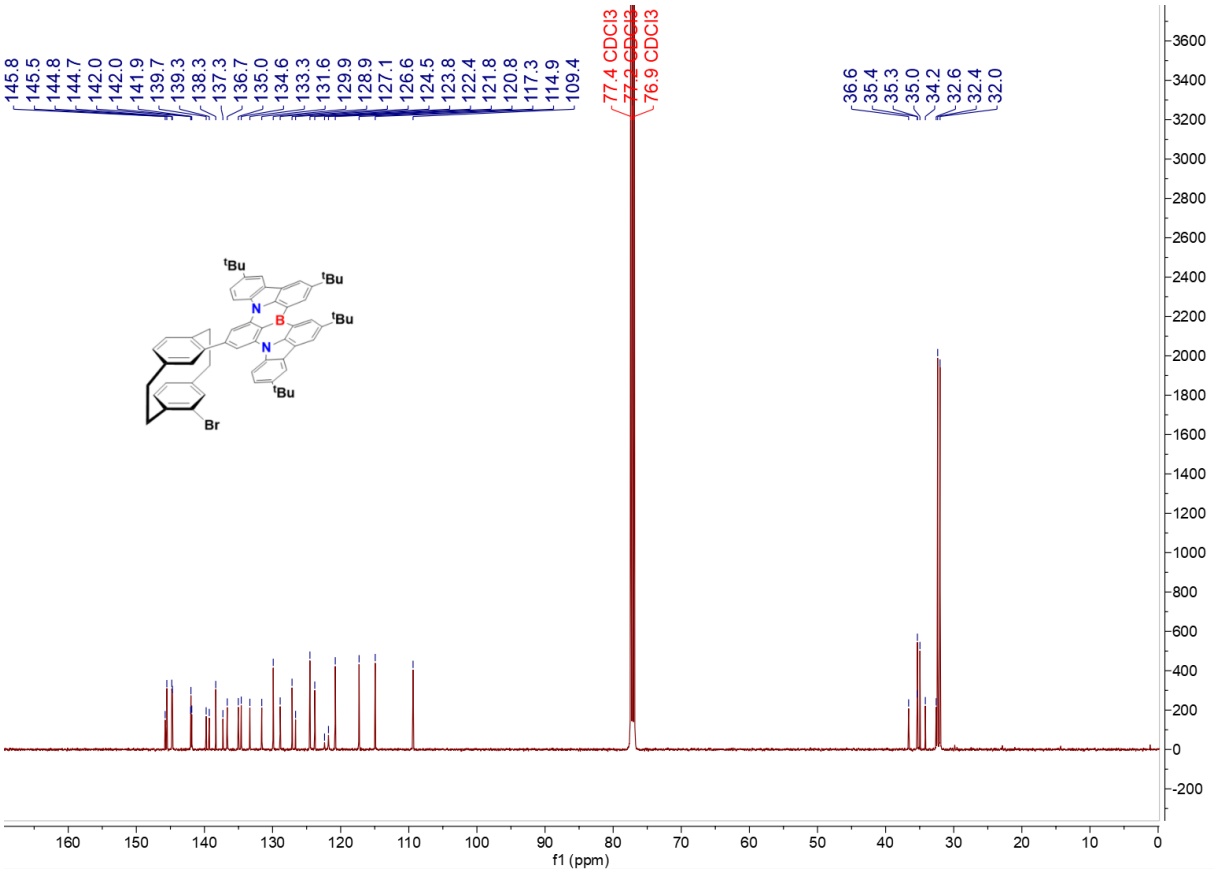

Figure **S7**. ^{13}C-NMR spectrum of ***po*-PCP-*t*CzBN-Br** in $CDCl_3$.

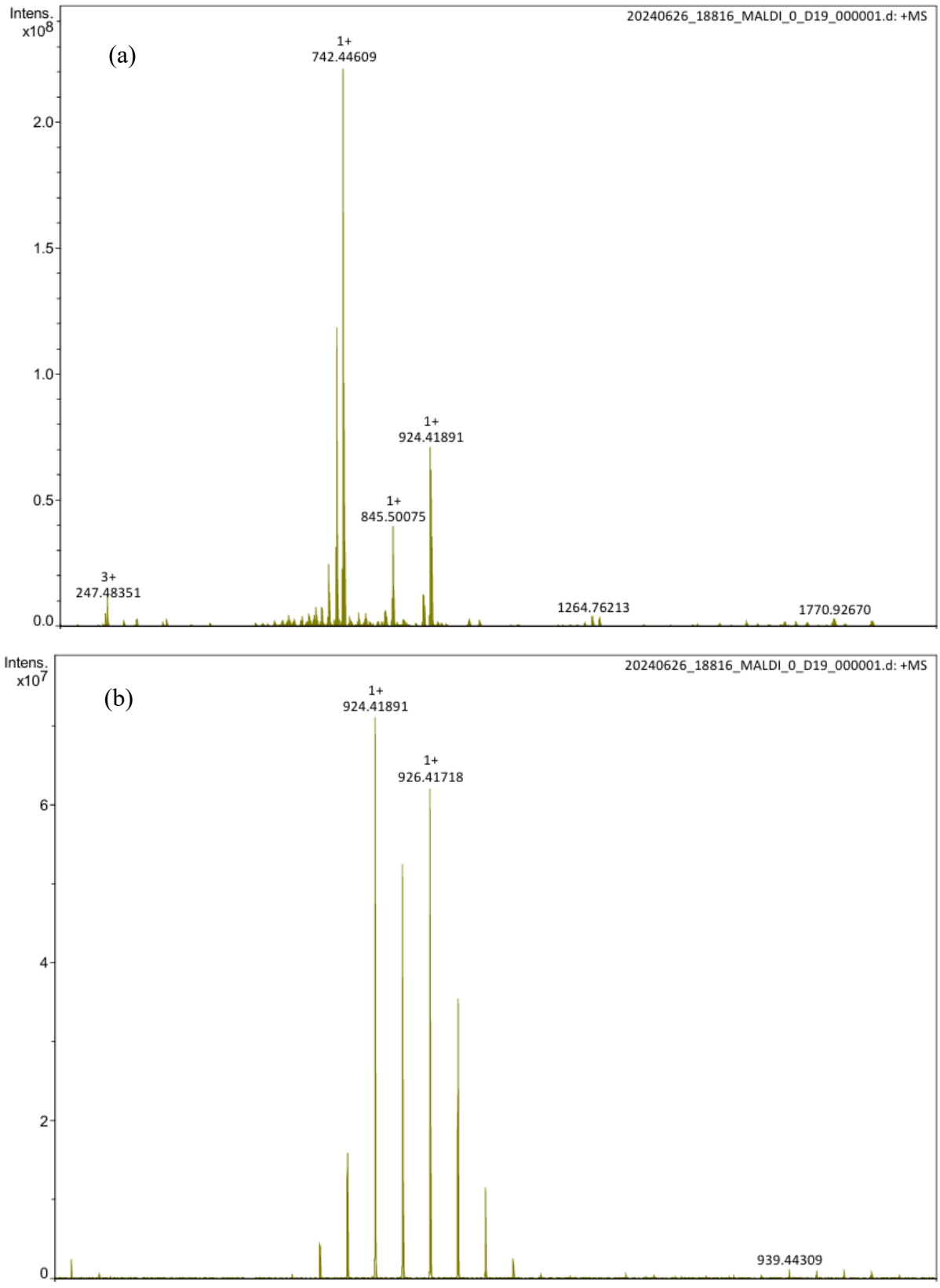

Figure **S8**. HRMS of ***po*-PCP-*t*CzBN-Br** (a) wide range spectrum, (b) **[M]**$^+$ ($C_{62}H_{62}BBrN_2$)

<Chromatogram>

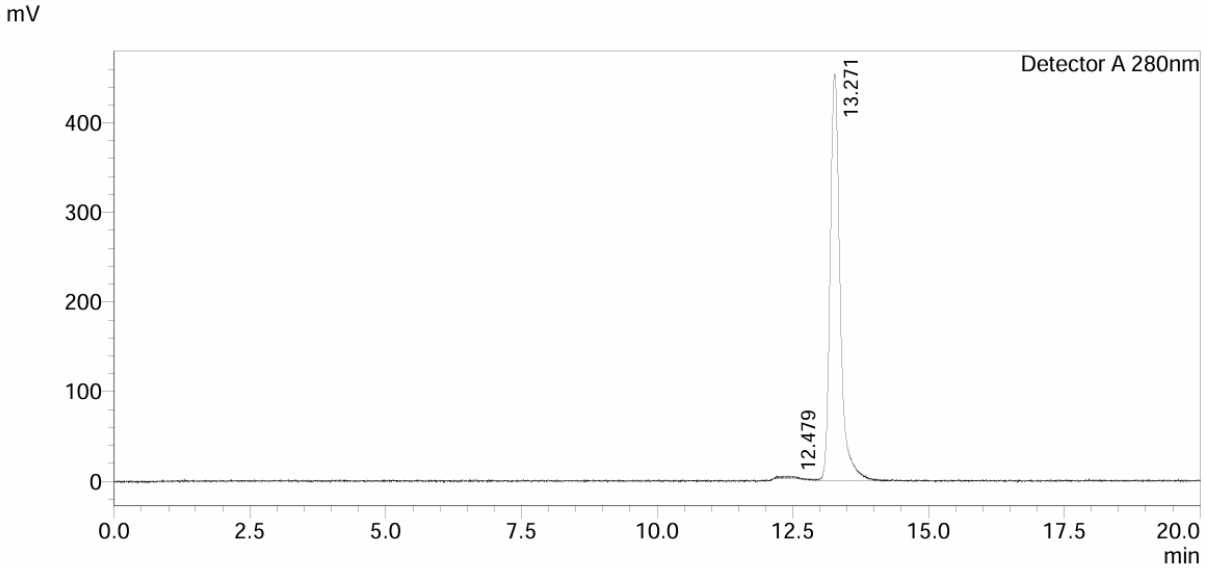

<Peak Table>

Detector A 280nm

Peak#	Ret. Time	Area	Height	Area%	Area/Height	Width at 5% Height
1	12.479	51495	2443	0.877	21.082	0.456
2	13.271	5820924	453494	99.123	12.836	0.490
Total		5872419	455937	100.000		

Figure **S9**. HPLC report of ***po*-PCP-*t*CzBN-Br**.

LONDON METROPOLITAN UNIVERSITY
HUMAN SCIENCES

Elemental Analysis Sample Results

Name	Yan Xu
Organisation Name	University of St Andrews
Purchase order number	P00032804

Standard – Acetanilide		
Element	**Expected %**	**Found**
Carbon	71.10 (+/- 0.23)	71.23
Hydrogen	6.71 (+/- 0.07)	6.71
Nitrogen	10.34 (+/- 0.09)	10.28

Analysis – poPCPtCzBNBr			
Element	**Expected %**	**Found (1)**	**Found (2)**
Carbon	80.43	80.31	80.13
Hydrogen	6.75	6.85	6.85
Nitrogen	3.03	2.78	2.79

Date completed	29.05.2025
Signature	O. McCullough
Comments	

Figure **S10**. EA results of ***po*-PCP-*t*CzBN-Br**.

Synthesis of *pm*-PCP-*t*CzBN-Br

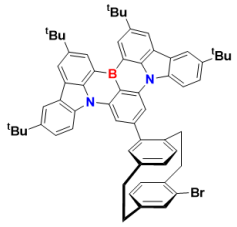

Under a N_2 atmosphere, a mixture of ***pm*-PCP-2Br** (215.0 mg, 0.6 mmol, 1.5 equiv.), ***t*CzBN-Bpin** (300.0 mg, 0.4 mmol, 1 equiv.), $Pd(PPh_3)_4$ (23.0 mg, 19.6 μmol, 0.05 equiv.), 2 M Na_2CO_3 (0.5 mL) and THF (10 mL) were combined. The reaction mixture was heated to reflux and stirred for 12 h. The reaction mixture was cooled to room temperature and the product was filtered and washed with water (3 × 50 mL) and dichloromethane (3 × 30 mL). The crude mixture was purified by silica gel flash column chromatography using dichloromethane: petroleum ether = 1:10 as eluent to afford the desired compound as yellow solid product. **Yield**: 42%. **Mp**: 284-287 °C. **R_f**: 0.5 (dichloromethane:petroleum ether = 1:5). **^{1}H NMR (500 MHz, $CDCl_3$) δ (ppm)**: 9.17 (d, *J* = 1.9 Hz, 2H), 8.51-8.48 (m, 4H), 8.46 (s, 2H), 8.31 (d, *J* = 2.1 Hz, 2H), 7.70 (dd, *J* = 8.8, 2.1 Hz, 2H), 7.49 (d, *J* = 7.8 Hz, 1H), 7.03-6.99 (m, 2H), 6.89 (dd, *J* = 7.9, 1.7 Hz, 1H), 6.81 (d, *J* = 1.7 Hz, 1H), 6.66 (dd, *J* = 7.8, 1.9 Hz, 1H), 3.85 (dd, *J* = 13.0, 10.2 Hz, 1H), 3.40 -3.30 (m, 3H), 3.26-3.17 (m, 2H), 3.11 (ddd, *J* = 13.1, 10.6, 5.1 Hz, 1H), 2.51 (ddd, *J* = 13.4, 9.9, 6.8 Hz, 1H), 1.69 (s, 18H), 1.55 (s, 18H). **^{13}C NMR (126 MHz, CD_2Cl_2) δ (ppm)**: 146.0, 145.6, 144.9, 144.7, 143.1, 142.0, 141.9, 140.0, 139.6, 138.5, 137.6, 137.2, 132.9, 132.4, 131.9, 130.4, 130.1, 127.6, 127.4, 124.6, 123.7, 121.8, 120.9, 117.7, 113.9, 109.5, 35.4, 35.4, 35.1, 35.0, 32.8, 32.4, 32.0. **HR-MS $[M]^+$ Calculated:** ($C_{62}H_{62}BBrN_2$) 924.42; **Found:** 924.42. **EA calculated:** ($C_{62}H_{62}BBrN_2$) C, 80.43%; H, 6.75%; N, 3.03%. **Found:** C, 79.75%; H, 6.83%; N, 2.74%. **HPLC purity:** > 99% (retention time: 13.245 minutes, employing an eluent of 100% THF).

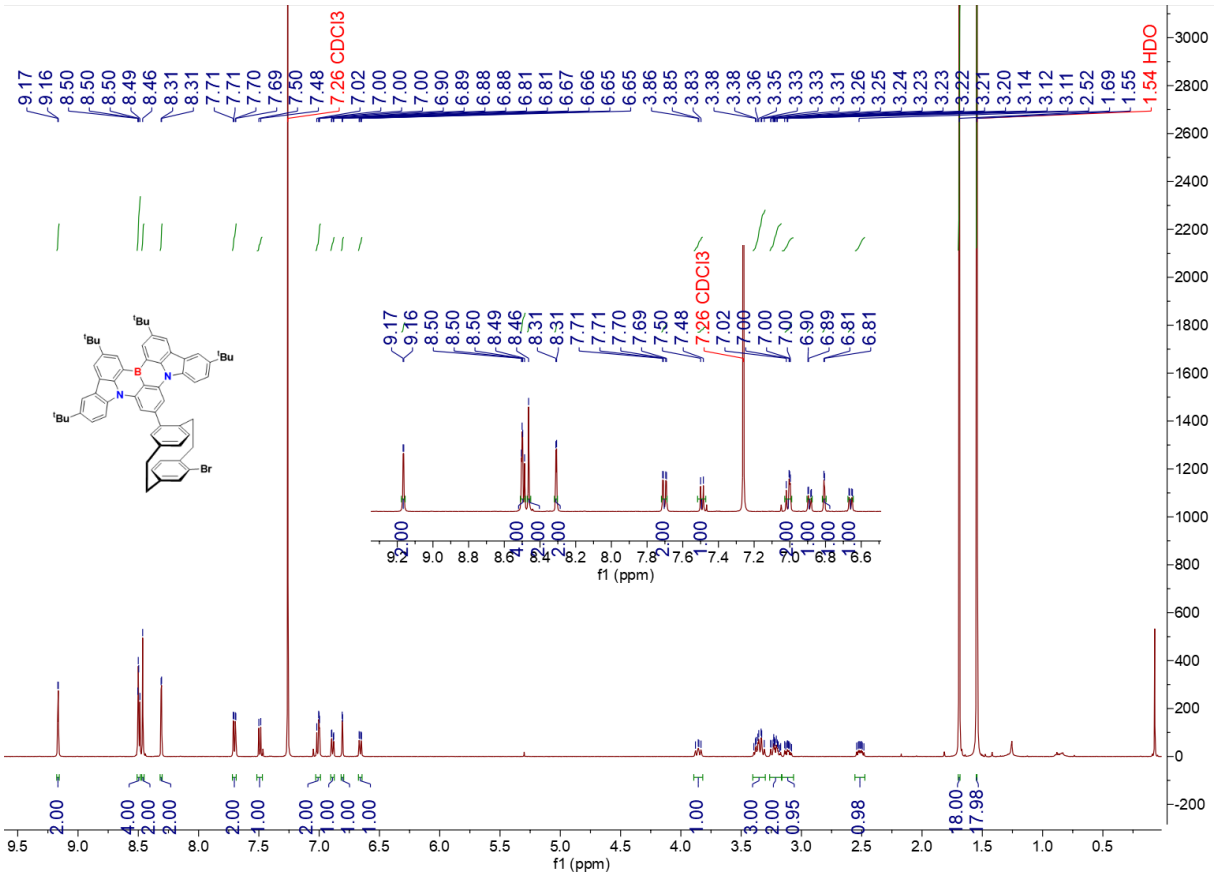

Figure **S11**. ^{1}H-NMR spectrum of ***pm*-PCP-*t*CzBN-Br** in $CDCl_3$.

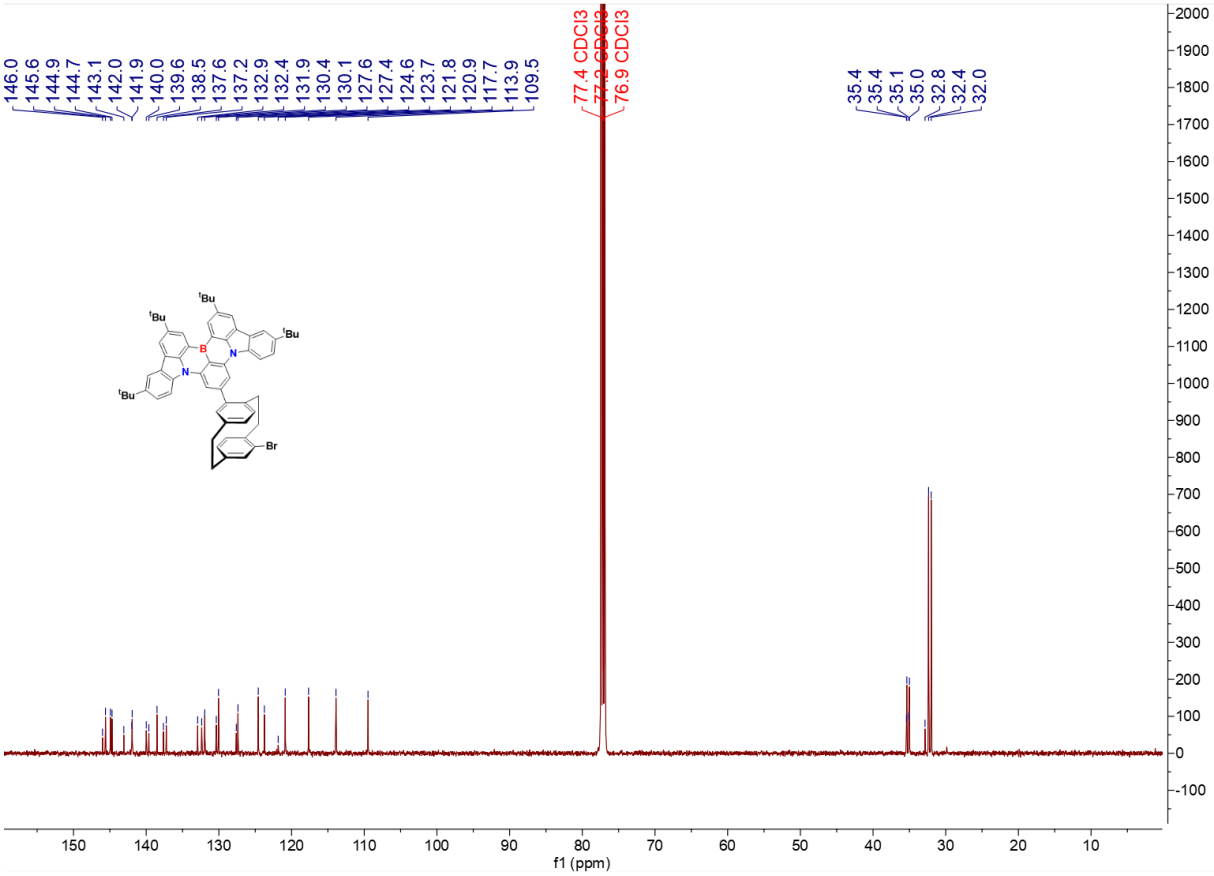

Figure **S12**. ^{13}C-NMR spectrum of ***pm*-PCP-*t*CzBN-Br** in $CDCl_3$.

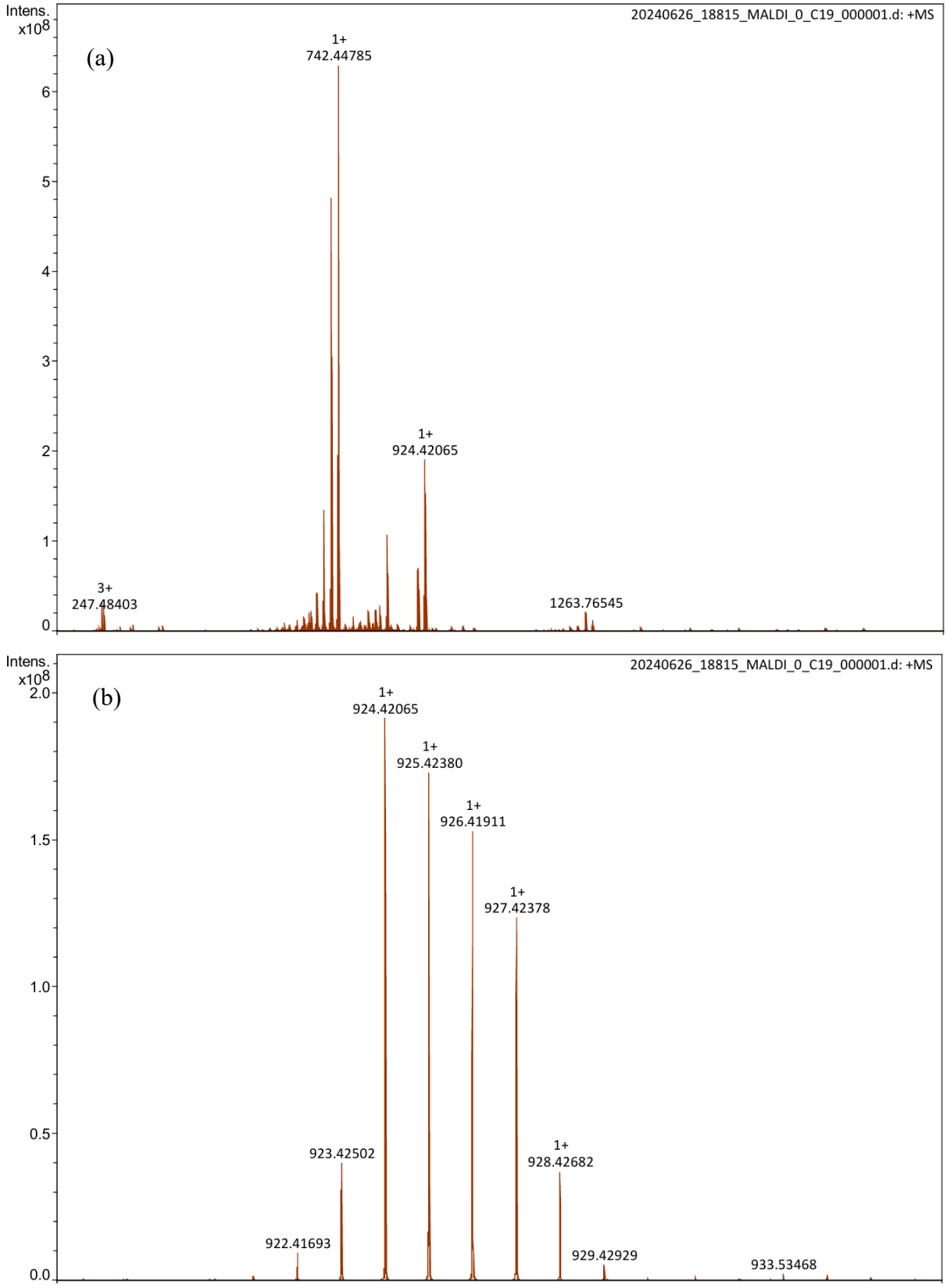

Figure **S13**. HRMS of ***pm*-PCP-*t*CzBN-Br** (a) wide range spectrum, (b) **[M]**$^+$ ($C_{62}H_{62}BBrN_2$)

<Chromatogram>

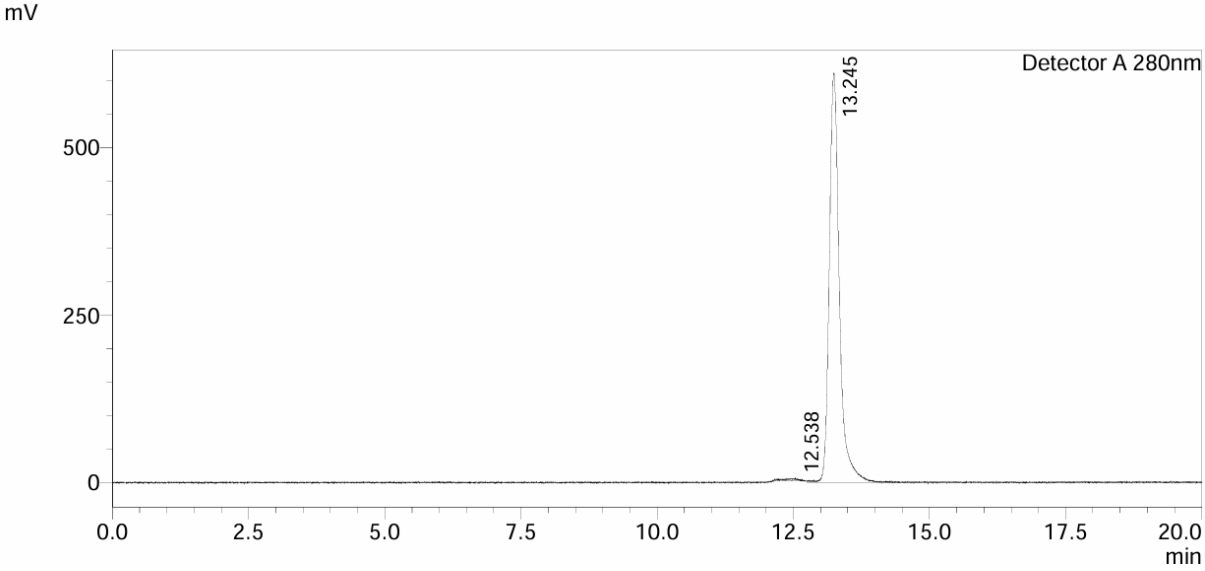

<Peak Table>

Detector A 280nm

Peak#	Ret. Time	Area	Height	Area%	Area/Height	Width at 5% Height
1	12.538	58649	2609	0.731	22.478	0.468
2	13.245	7960741	611062	99.269	13.028	0.493
Total		8019390	613671	100.000		

Figure **S14**. HPLC report of ***pm*-PCP-*t*CzBN-Br**.

LONDON METROPOLITAN UNIVERSITY
HUMAN SCIENCES

Elemental Analysis Sample Results

Name	Yan Xu
Organisation Name	University of St Andrews
Purchase order number	

Standard – Acetanilide		
Element	**Expected %**	**Found**
Carbon	71.10 (+/- 0.23)	71.33
Hydrogen	6.71 (+/- 0.07)	6.68
Nitrogen	10.34 (+/- 0.09)	10.42

Analysis – PCPtCzBNBrmeta			
Element	**Expected %**	**Found (1)**	**Found (2)**
Carbon	80.43	79.94	79.55
Hydrogen	6.75	6.82	6.83
Nitrogen	3.03	2.74	2.74

Date completed	18.11.2024
Signature	O. McCullough
Comments	

Figure **S15**. EA results of ***pm*-PCP-*t*CzBN-Br**.

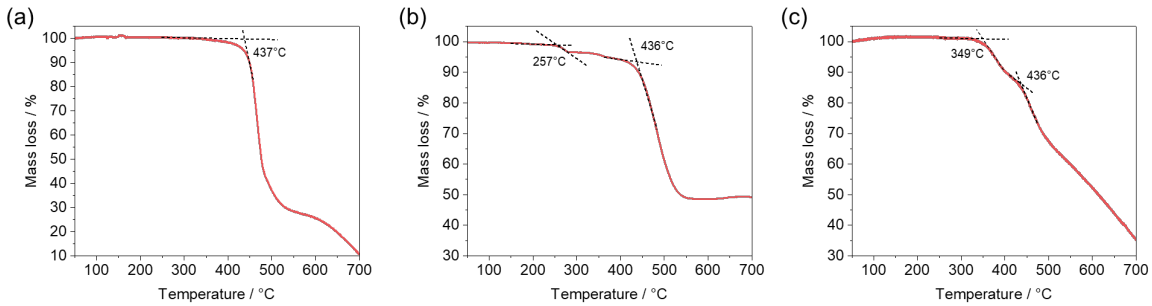

Figure **S16**. TGA traces of (a) **PCP-*t*CzBN**, (b) ***po*-PCP-*t*CzBN-Br** and (c) ***pm*-PCP-*t*CzBN-Br**.

3. Theoretical and optoelectronic data

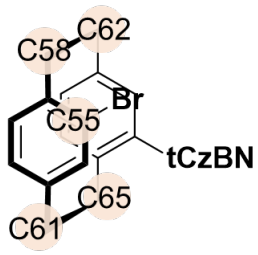

Figure **S17**. The structure illustration of the bonds considered for BDE comparison.

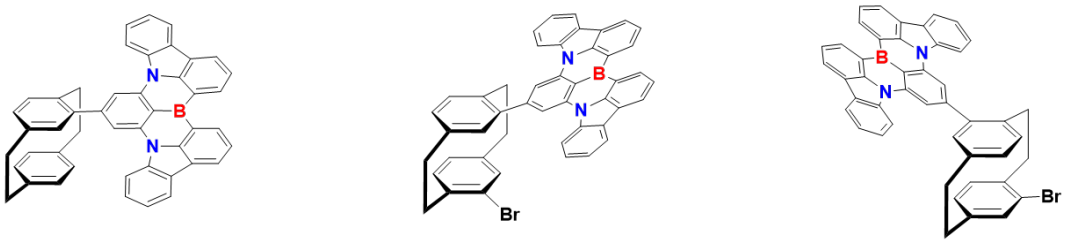

Figure **S18**. The structures of the model compounds **PCP-CzBN**, ***po*-PCP-CzBN-Br** and ***pm*-PCP-CzBN-Br** in the DFT study where the *tert*-butyl groups have been omitted.

Table **S1**. BDE calculations.[a]

Reactant energy / hartree	Fragment energy / hartree		BDE / hartree	BDE / kcal• mol^{-1}
***po*-PCP-*t*CzBN-Br** -4474.1	***po*-PCP-*t*CzBN•** -1902.6	**Br•** -2571.3	0.16	100
	***po*-PCP-*t*CzBN-Br C58• C62•** -4474.0		0.06	38
	***po*-PCP-*t*CzBN-Br C61• C65•** -4474.0		0.06	38

[a] Calculated at the PBE0/6-31G(d,p) level in the gas phase at the optimized ground-state geometry.

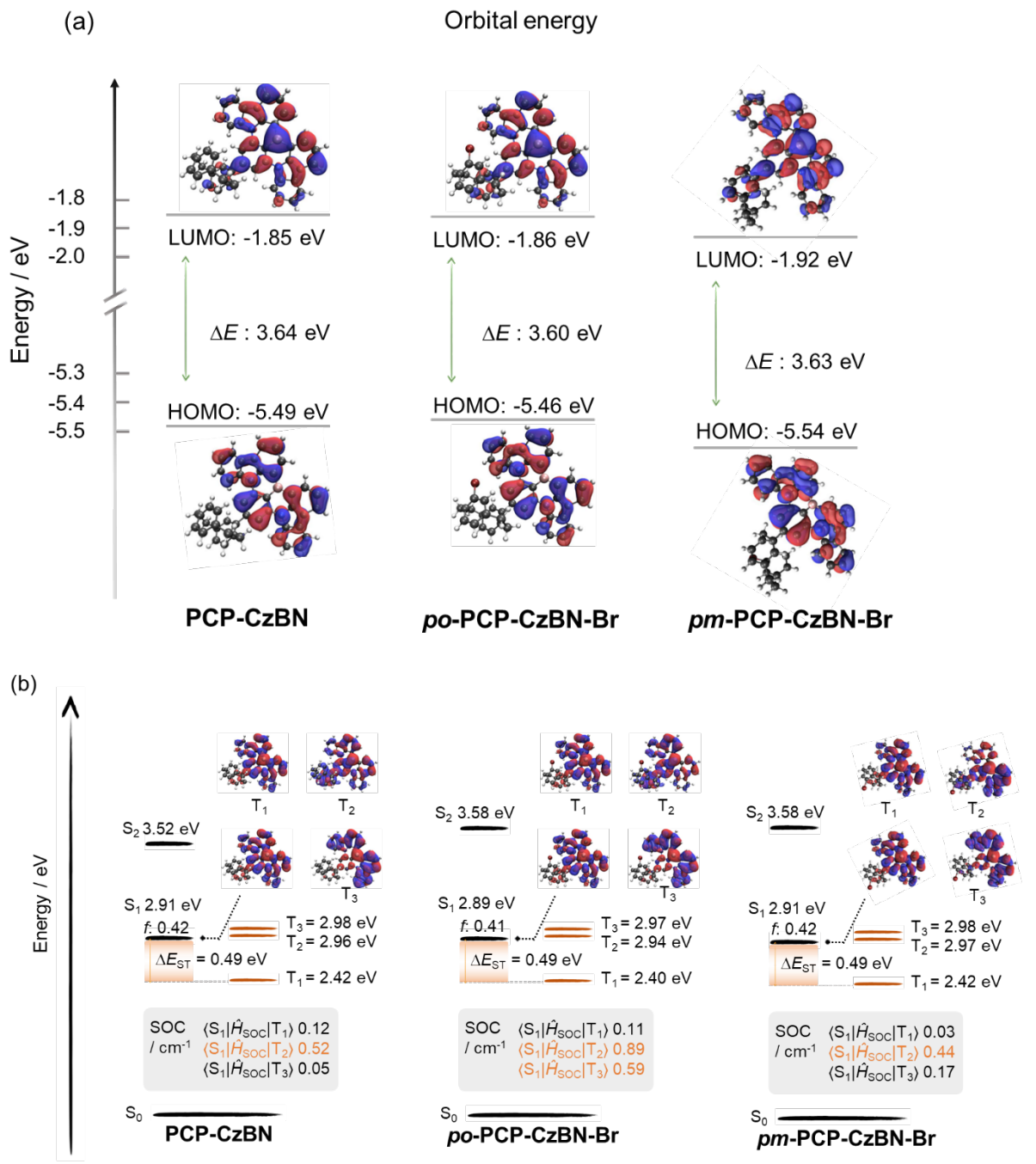

Figure **S19**. Theoretical modeling of **PCP-CzBN**, ***po*-PCP-CzBN-Br** and ***pm*-PCP-CzBN-Br** in the gas phase at the PBE0/6-31G(d,p) level. (a) the energies and electron density distributions of the HOMO/LUMO (ISO value = 0.02); (b) NTOs (particle and hole are represented by red and blue colors, respectively), the associated vertical excitation energies, SOC between the singlet state and triplet states computed based on the optimized T_1 geometries at the PBE0/6-31G(d,p) level for **PCP-CzBN**, ***po*-PCP-CzBN-Br** and ***pm*-PCP-CzBN-Br**. *f* is the oscillator strength.

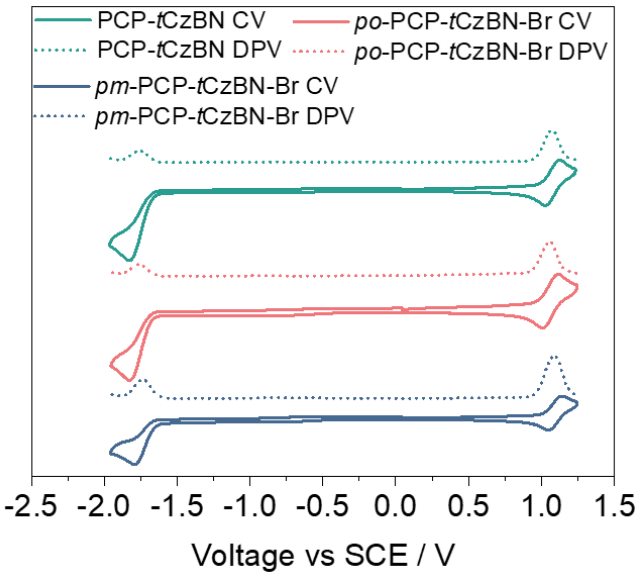

Figure **S20**. CVs and DPVs of **PCP-*t*CzBN, *po*-PCP-*t*CzBN-Br** and ***pm*-PCP-*t*CzBN-Br** in deaerated DCM with 0.1 M [^{n}Bu$_4$N]PF$_6$ as the supporting electrolyte and Fc/Fc$^+$ as the internal reference (0.46 V vs. SCE).[4]

Table **S2**. Electrochemical data.

	E_{ox} [a] / v *vs* SCE	E_{red} [a] / v *vs* SCE	HOMO[b] / eV	LUMO[b] / eV	ΔE_{redox} [c] / eV
PCP-*t*CzBN	1.07	-1.76	-5.41	-2.58	2.83
***po*-PCP-*t*CzBN-Br**	1.06	-1.76	-5.40	-2.58	2.82
***pm*-PCP-*t*CzBN-Br**	1.09	-1.74	-5.43	-2.60	2.83

[a] Measured in DCM (0.46 V for DCM *vs* SCE[4]) with a scan rate of 0.1 V/s. [b] The HOMO and LUMO energies were determined using $E_{HOMO/LUMO}$ = - (E_{ox}/E_{red}+4.8) eV[5] where E_{ox} and E_{red} are anodic and cathodic peak potentials, respectively, versus Fc/Fc$^+$. [c] $\Delta E_{redox} = |E_{HOMO}-E_{LUMO}|$.

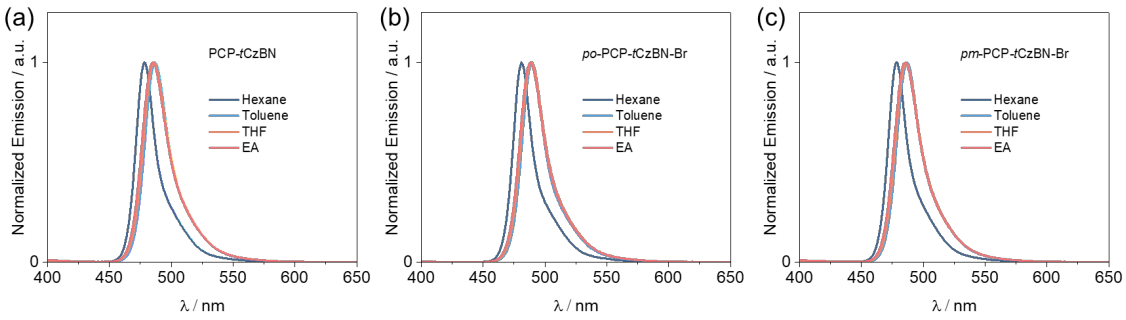

Figure **S21**. Steady-state PL spectra in different solvents of (a) **PCP-*t*CzBN**, (b) ***po*-PCP-*t*CzBN-Br** and (c) ***pm*-PCP-*t*CzBN-Br** (λ_{exc} = 325 nm).

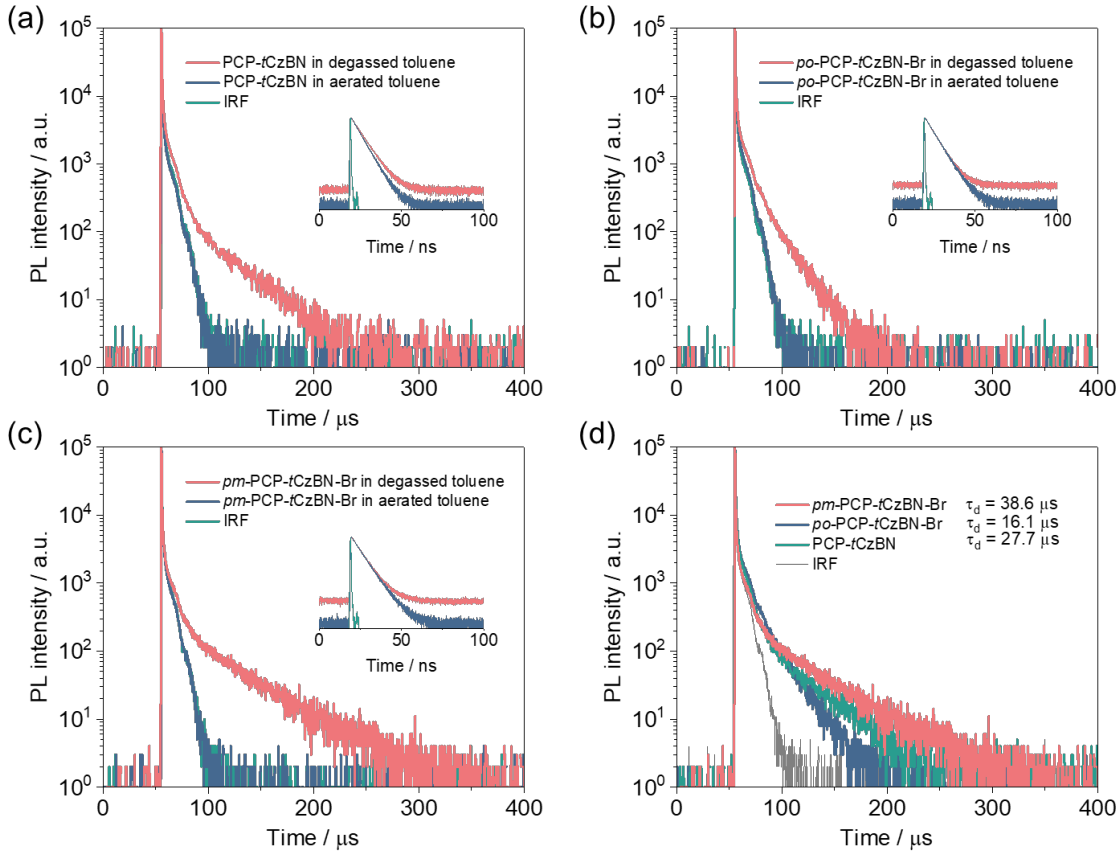

Figure **S22**. Time-resolved PL decays (λ_{exc} = 375 nm) in toluene for (a) **PCP-*t*CzBN**, (b) ***po*-PCP-*t*CzBN-Br**, (c) ***pm*-PCP-*t*CzBN-Br** and (d) three emitters in comparison at room temperature (inset figures are the time-resolved PL decays of the prompt component, λ_{exc} = 375 nm).

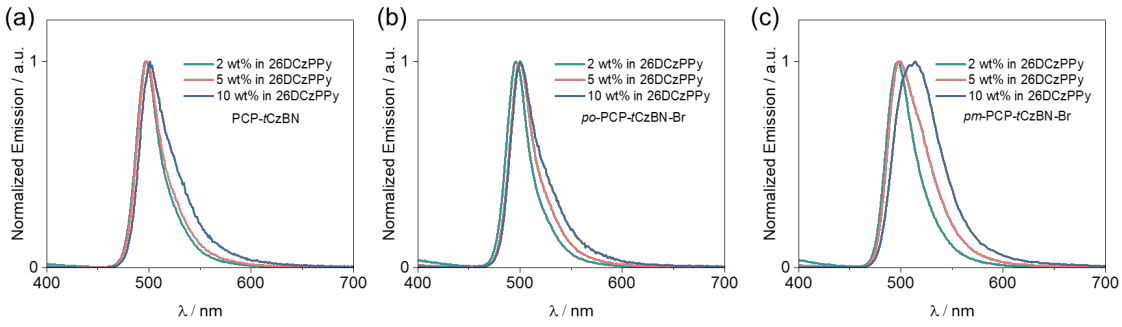

Figure **S23**. Steady-state PL spectra of (a) **PCP-*t*CzBN**, (b) ***po*-PCP-*t*CzBN-Br** and (c) ***pm*-PCP-*t*CzBN-Br** doped 26DCzPPy films at different concentrations (λ_{exc} = 340 nm).

Table **S3**. Photoluminescence quantum yield screening at different doping concentrations of **PCP-*t*CzBN** in spin-coated 26DCzPPy thin films[a]

	2 wt%	**5 wt%**	**10 wt%**
In N_2	84	81	50
In air	74	71	46

[a] Φ_{PL} values were determined using an integrating sphere (λ_{exc} = 340 nm); degassing was done by N_2 purge for 2 minutes.

Table **S4**. Photoluminescence quantum yield screening at different doping concentrations of ***po*-PCP-*t*CzBN-Br** in spin-coated 26DCzPPy thin films[a]

	2 wt%	**5 wt%**	**10 wt%**
In N_2	84	81	50
In air	73	71	46

[a] Φ_{PL} values were determined using an integrating sphere (λ_{exc} = 340 nm); degassing was done by N_2 purge for 2 minutes.

Table **S5**. Photoluminescence quantum yield screening at different doping concentrations of ***pm*-PCP-*t*CzBN-Br** in spin-coated 26DCzPPy thin films[a]

	2 wt%	**5 wt%**	**10 wt%**
In N_2	90	77	50
In air	70	63	43

[a] Φ_{PL} values were determined using an integrating sphere (λ_{exc} = 340 nm); degassing was done by N_2 purge for 2 minutes.

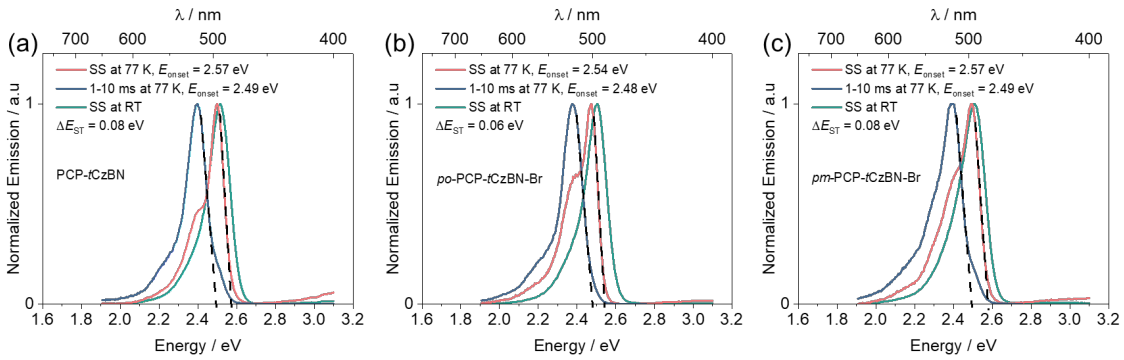

Figure **S24**. SS PL spectra of **PCP-*t*CzBN** (a)**, *po*-PCP-*t*CzBN-Br** (b) **and *pm*-PCP-*t*CzBN-**

Br (c) at 77 K and room temperature (λ_{exc} = 340 nm), and phosphorescence spectra at 77 K (1-10 ms, λ_{exc} = 340 nm) in 2 wt% doped films in 26DCzPPy.

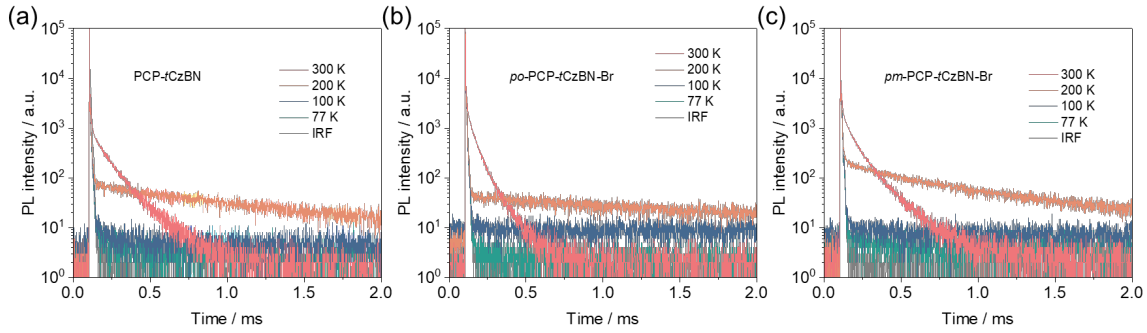

Figure **S25**. Temperature-dependent time-resolved PL decay of 2 wt% doped films of (a) **PCP-*t*CzBN**, (b) ***po*-PCP-*t*CzBN-Br** and (c) ***pm*-PCP-*t*CzBN-Br** in 26DCzPPy. λ_{exc} = 375 nm.

4. Kinetics parameters

The kinetics parameters were calculated according to the following equations and summarized in Table **S5**.[33, 34]

$\Phi_{PL} = \Phi_p + \Phi_d$ (1)

$k_p = \frac{1}{\tau_p}$ (2)

$k_d = \frac{1}{\tau_d}$ (3)

$k_r^S = k_p \Phi_p$ (4)

$k_{ISC} = k_p(1-\Phi_p)$ (5)

$k_{RISC} = \frac{k_p k_d}{k_{ISC}} \frac{\Phi_d}{\Phi_p}$ (6)

$k_{nr}^T = k_d - \Phi_p k_{RISC}$ (7)

where the Φ_p and Φ_d are the prompt fluorescent and delayed fluorescent quantum efficiencies, respectively. The overall photoluminescence quantum efficiency was measured using an integrating sphere of the emission from the 2 wt% spin-coated doped films in 26DCzPPy, and the Φ_p and Φ_d were determined as the fraction of prompt and delayed emission based on the ratio of prompt and delayed components obtained from the integration of their time-resolved PL decays; k_p is the rate constant of prompt fluorescence; k_d is the rate constant of delayed fluorescence; k^T_{nr} is the non-radiative decay rate constant of T_1; k^S_r is the radiative decay rate constant of S_1; k_{ISC} is the intersystem crossing rate constant; k_{RISC} is the reverse intersystem crossing rate constant.

Table **S6**. Summary of kinetics parameters for **PCP-*t*CzBN**, ***po*-PCP-*t*CzBN-Br** and ***pm*-PCP-*t*CzBN-Br** in degassed toluene

	Φ_p / %	Φ_d / %	k_p / 10^8 s^{-1}	k_d / 10^4 s^{-1}	k^T_{nr} / 10^4 s^{-1}	k^S_r / 10^8 s^{-1}	k_{ISC} / 10^7 s^{-1}	k_{RISC} / 10^4 s^{-1}
PCP-*t*CzBN	70	4	1.84	3.61	3.13	1.29	5.52	0.69
***po*-PCP-*t*CzBN-Br**	65	8	2.02	6.21	4.76	1.31	7.12	2.24
***pm*-PCP-*t*CzBN-Br**	84	11	1.81	2.59	0.79	1.51	2.98	2.16

Table **S7**. Summary of kinetics parameters measured from spin-coated 2 wt% doped thin films in 26DCzPPy.

	Φ_p / %	Φ_d / %	k_p / 10^8 s^{-1}	k_d / 10^4 s^{-1}	k^T_{nr} / 10^3 s^{-1}	k^S_r / 10^7 s^{-1}	k_{ISC} / 10^8 s^{-1}	k_{RISC} / 10^4 s^{-1}
PCP-*t*CzBN	42	42	1.75	1.60	4.38	7.30	1.02	2.79
***po*-PCP-*t*CzBN-Br**	36	48	1.96	2.50	6.20	6.96	1.26	5.29
***pm*-PCP-*t*CzBN-Br**	39	51	1.82	1.92	3.14	7.08	1.11	4.12

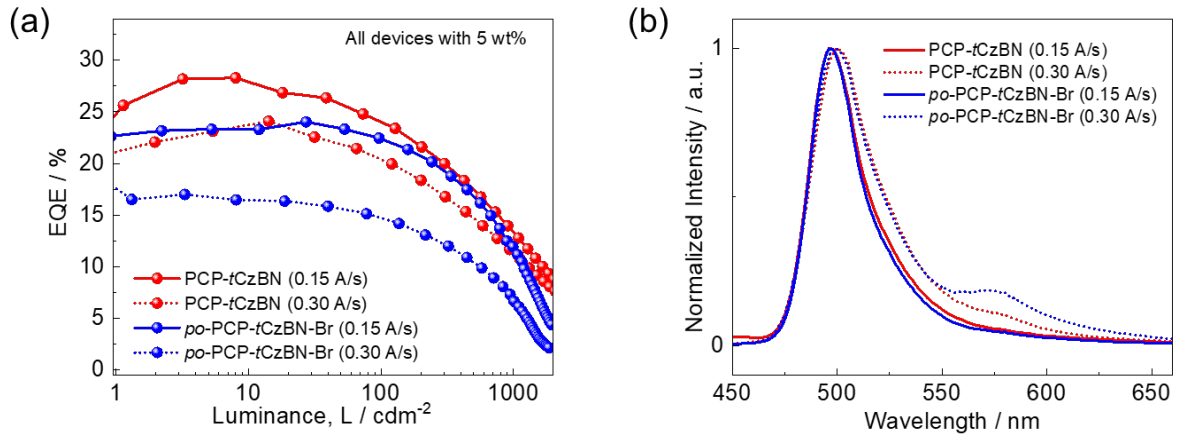

Figure **S26**. (a) EQE vs luminance; (b) Electroluminescence spectra for **PCP-*t*CzBN** and ***po*-PCP-*t*CzBN-Br** at different evaporation rates.

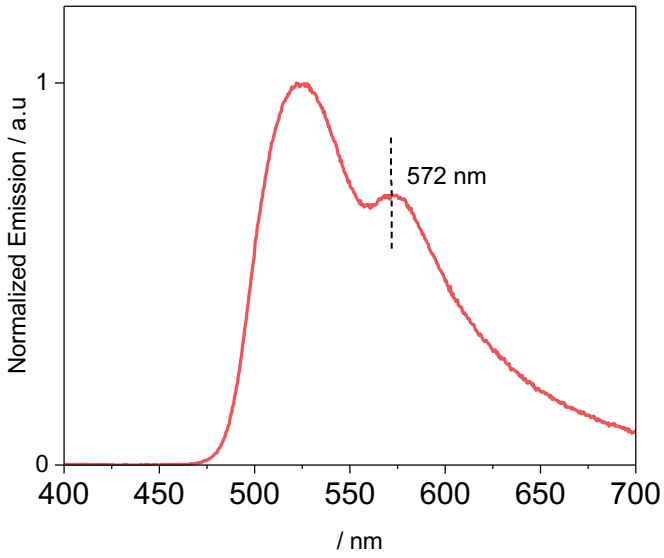

Figure **S27**. Steady-state PL spectra of the neat film of ***po*-PCP-*t*CzBN-Br** (λ_{exc} = 340 nm).

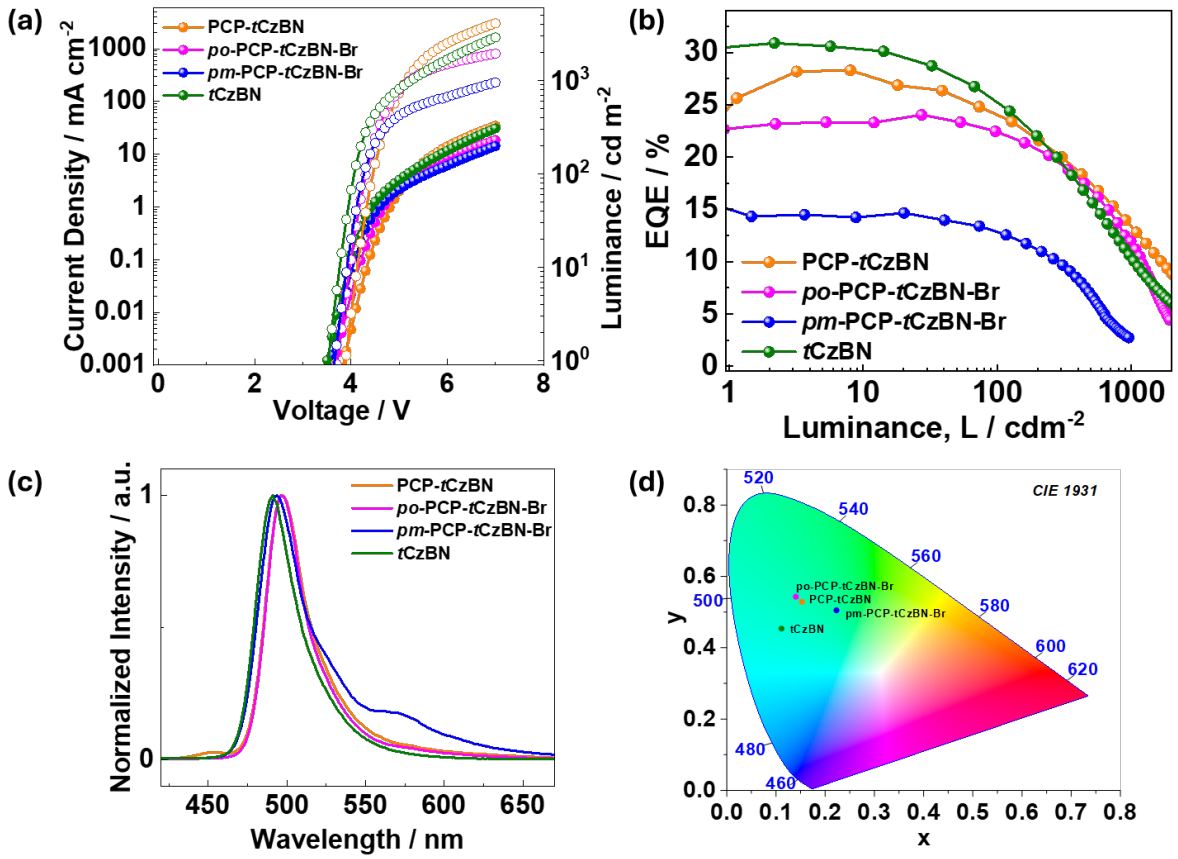

Figure **S28**. Device performance of OLEDs using 5 wt% of the emitters. (a) Current density (solid circles)-voltage-luminance (hollow circles) (JVL) characteristics; (b) EQE vs luminance; (c) Electroluminescence spectra; (d) CIE coordinates of the devices.

References

1. N. Sharma, E. Spuling, Cornelia M. Mattern, W. Li, O. Fuhr, Y. Tsuchiya, C. Adachi, S. Bräse, I. D. W. Samuel and E. Zysman-Colman, Turn on of sky-blue thermally activated delayed fluorescence and circularly polarized luminescence (CPL) via increased torsion by a bulky carbazolophane donor, *Chem. Sci.*, 2019, **10**, 6689-6696.
2. H. Hopf, L. Bondarenko, I. Dix and H. Hinrichs, Cyclophanes. Part LII: ethynyl[2.2]paracyclophanes - new building blocks for molecular scaffolding, *Synth.*, 2004, **2004**, 2751-2759.
3. Y. Xu, C. Li, Z. Li, J. Wang, J. Xue, Q. Wang, X. Cai and Y. Wang, Highly efficient electroluminescent materials with high color purity based on strong acceptor attachment onto B-N-containing multiple resonance frameworks, *CCS Chem.*, 2022, **4**, 2065-2079.
4. N. G. Connelly and W. E. Geiger, Chemical redox agents for organometallic chemistry, *Chem. Rev.*, 1996, **96**, 877-910.
5. C. M. Cardona, W. Li, A. E. Kaifer, D. Stockdale and G. C. Bazan, Electrochemical considerations for determining absolute frontier orbital energy levels of conjugated polymers for solar cell applications, *Adv. Mater.*, 2011, **23**, 2367-2371.
6. M. J. Frisch, G. W. Trucks, H. B. Schlegel, G. E. Scuseria, M. A. Robb, J. R. Cheeseman, G. Scalmani, V. Barone, G. A. Petersson, H. Nakatsuji, X. Li, M. Caricato, A. V. Marenich, J. Bloino, B. G. Janesko, R. Gomperts, B. Mennucci, H. P. Hratchian, J. V. Ortiz, A. F. Izmaylov, J. L. Sonnenberg, Williams, F. Ding, F. Lipparini, F. Egidi, J. Goings, B. Peng, A. Petrone, T. Henderson, D. Ranasinghe, V. G. Zakrzewski, J. Gao, N. Rega, G. Zheng, W. Liang, M. Hada, M. Ehara, K. Toyota, R. Fukuda, J. Hasegawa, M. Ishida, T. Nakajima, Y. Honda, O. Kitao, H. Nakai, T. Vreven, K. Throssell, J. A. Montgomery Jr., J. E. Peralta, F. Ogliaro, M. J. Bearpark, J. J. Heyd, E. N. Brothers, K. N. Kudin, V. N. Staroverov, T. A. Keith, R. Kobayashi, J. Normand, K. Raghavachari, A. P. Rendell, J. C. Burant, S. S. Iyengar, J. Tomasi, M. Cossi, J. M. Millam, M. Klene, C. Adamo, R. Cammi, J. W. Ochterski, R. L. Martin, K. Morokuma, O. Farkas, J. B. Foresman, D. J. Fox, Wallingford, CT 2016.
7. C. Adamo and V. Barone, Toward reliable density functional methods without adjustable parameters: The PBE0 model, *J. Chem. Phys.*, 1999, **110**, 6158-6170.
8. G. A. Petersson and M. A. Al-Laham, A complete basis set model chemistry. II. Open-shell systems and the total energies of the first-row atoms, *J. Chem. Phys.*, 1991, **94**, 6081-6090.
9. S. Hirata and M. Head-Gordon, Time-dependent density functional theory within the Tamm-Dancoff approximation, *Chem. Phys. Lett.*, 1999, **314**, 291-299.
10. X. Gao, S. Bai, D. Fazzi, T. Niehaus, M. Barbatti and W. Thiel, Evaluation of spin-orbit couplings with linear-response time-dependent density functional methods, *J. Chem. Theory Comput.*, 2017, **13**, 515-524.
11. R. Dennington, T. A. Keith and J. M. Millam, *GaussView, Version 6*, Semichem Inc., Shawnee Mission, KS, 2016.
12. *TURBOMOLE V7.5 2020, a development of University of Karlsruhe and*

Forschungszentrum Karlsruhe GmbH, 1989-2007, 7.5; TURBOMOLE GmbH, since 2007; available from https://www.turbomole.org: 2020.

13. S. G. Balasubramani, G. P. Chen, S. Coriani, M. Diedenhofen, M. S. Frank, Y. J. Franzke, F. Furche, R. Grotjahn, M. E. Harding, C. Hattig, A. Hellweg, B. Helmich-Paris, C. Holzer, U. Huniar, M. Kaupp, A. Marefat Khah, S. Karbalaei Khani, T. Muller, F. Mack, B. D. Nguyen, S. M. Parker, E. Perlt, D. Rappoport, K. Reiter, S. Roy, M. Ruckert, G. Schmitz, M. Sierka, E. Tapavicza, D. P. Tew, C. van Wullen, V. K. Voora, F. Weigend, A. Wodynski and J. M. Yu, TURBOMOLE: Modular program suite for ab initio quantum-chemical and condensed-matter simulations, *J. Chem. Phys.*, 2020, **152**, 184107.
14. C. Hättig and F. Weigend, CC2 excitation energy calculations on large molecules using the resolution of the identity approximation, *J. Chem. Phys.*, 2000, **113**, 5154-5161.
15. A. Hellweg, S. A. Grün and C. Hättig, Benchmarking the performance of spin-component scaled CC2 in ground and electronically excited states, *Phys. Chem. Chem. Phys.*, 2008, **10**, 4119-4127.
16. J. Schirmer, Beyond the random-phase approximation: A new approximation scheme for the polarization propagator, *Phys. Rev. A*, 1982, **26**, 2395-2416.
17. A. B. Trofimov and J. Schirmer, An efficient polarization propagator approach to valence electron excitation spectra, *J. Phys. B: At. Mol. Opt. Phys.*, 1995, **28**, 2299-2324.
18. T. H. Dunning, Jr., Gaussian basis sets for use in correlated molecular calculations. I. The atoms boron through neon and hydrogen, *J. Chem. Phys.*, 1989, **90**, 1007-1023.
19. C. Hättig and A. Köhn, Transition moments and excited-state first-order properties in the coupled-cluster model CC2 using the resolution-ofthe-identity approximation, *J. Chem. Phys.*, 2002, **117**, 6939-6951.
20. C. Hättig and K. Hald, Implementation of RI-CC2 triplet excitation energies with an application to trans-azobenzene, *Phys. Chem. Chem. Phys.*, 2002, **4**, 2111-2118.
21. C. Hättig, A. Köhn and K. Hald, First-order properties for triplet excited states in the approximated coupled cluster model CC2 using an explicitly spin coupled basis, *J. Chem. Phys.*, 2002, **116**, 5401-5410.
22. O. S. Lee and E. Zysman-Colman, *Digichem (version 6) InSilico Computing*, St Andrews, Scotland, 2024.
23. O. Lee, M. Gather and E. Zysman-Colman, Digichem: Computational Chemistry For Everyone, *Digit. Discov.*, 2024, **3**, 1695-1713.
24. N. M. O'boyle, A. L. Tenderholt and K. M. Langner, Cclib: a library for package-independent computational chemistry algorithms, *J. Comput. Chem*, 2008, **29**, 839-845.
25. W. Humphrey, A. Dalke and K. Schulten, VMD: visual molecular dynamics, *J. Mol. Graph.*, 1996, **14**, 33-38.
26. J. E. Stone, *An efficient library for parallel ray tracing and animation*, 1998.
27. J. D. Hunter, Matplotlib: A 2D graphics environment, *Comput. Sci. Eng.*, 2007, **9**, 90-95.
28. N. M. O'Boyle, M. Banck, C. A. James, C. Morley, T. Vandermeersch and G. R. Hutchison, Open Babel: An open chemical toolbox, *J. Cheminform*, 2011, **3**, 1-14.
29. N. M. O'Boyle and G. R. Hutchison, Cinfony-combining Open Source cheminformatics toolkits behind a common interface, *Chem. Cent. J.*, 2008, **2**, 24.

30. G. A. Crosby and J. N. Demas, Measurement of photoluminescence quantum yields. Review, *J. Phys. Chem.*, 1971, **75**, 991-1024.
31. A. M. Brouwer, Standards for photoluminescence quantum yield measurements in solution (IUPAC Technical Report), *Pure Appl. Chem.* 2011, **83**, 2213-2228.
32. Y. Xu, D. Chen, S. Wu, D. Black, H. Wang, R. Pal, X. Zhang and E. Zysman-Colman, Accelerating reverse intersystem crossing by bridging two multiresonant thermally activated delayed fluorescence emitters with [2.2]paracyclophane, *CCS Chem.*, 2025, **7**, 3635-3649.
33. K. Masui, H. Nakanotani and C. Adachi, Analysis of exciton annihilation in high-efficiency sky-blue organic light-emitting diodes with thermally activated delayed fluorescence, *Org. Electron.*, 2013, **14**, 2721-2726.
34. Y. Tsuchiya, S. Diesing, F. Bencheikh, Y. Wada, P. L. Dos Santos, H. Kaji, E. Zysman-Colman, I. D. W. Samuel and C. Adachi, Exact solution of kinetic analysis for thermally activated delayed fluorescence materials, *J. Phys. Chem. A.*, 2021, **125**, 8074-8089.